

# **Mechanical properties and plasticity size effect of Fe-6%Cr irradiated by Fe ions and by neutrons**

C.D. Hardie<sup>a,b</sup>, G.R. Odette<sup>c</sup>, Y. Wu<sup>c</sup>, S. Akhmaliev<sup>d</sup> and S.G. Roberts<sup>a,b</sup>

<sup>a</sup> EURATOM/CCFE Association, Culham Centre for Fusion Energy (CCFE), Abingdon, Oxfordshire OX14 3DB, United Kingdom

<sup>b</sup> Department of Materials, University of Oxford, Oxford, OX1 3PH, United Kingdom

<sup>c</sup> UCSB Department of Mechanical Engineering, 2343 Engineering II Building, Santa Barbara, CA 93106-5070, United States of America

<sup>d</sup> Helmholtz-Zentrum Dresden-Rossendorf, Institute of Ion Beam Physics and Materials Research, D-01328 Dresden, Germany

Name: Christopher Hardie

Address: Culham Centre for Fusion Energy (CCFE),  
Abingdon,  
Oxfordshire,  
OX14 3DB,  
United Kingdom

Telephone Number: +44 (0)1235 46 4736

Email Address: chris.hardie@ukaea.uk

Manuscript Number: JNM-D-16-00574R1

Title: Mechanical properties and plasticity size effect of Fe-6%Cr  
irradiated by Fe ions and by neutrons

Article Type: Full Length Article

Section/Category: Basic science of radiation effects

Corresponding Author: Dr. Christopher D. Hardie, PhD

Corresponding Author's Institution:

First Author: Christopher D. Hardie, PhD

Order of Authors: Christopher D. Hardie, PhD; George R Odette; Shavkat  
Akhmadaliev; Yuan Wu; Steve Roberts

**Abstract:** This study compares the effects of ion and neutron irradiation on Fe 6%Cr irradiated to the same dose and at the same temperature by these two methods, and compared with unirradiated material. In recent work reported elsewhere, the materials were characterised by Transmission Electron Microscopy (TEM) and Atom Probe Tomography (APT). This paper reports further investigation of the alloy using nanoindentation and micromechanical testing. Irradiated and un-irradiated micro-cantilevers with a wide range of dimensions were used to study the interrelationships between irradiation hardening and size effects in small-scale plasticity. TEM and APT results identified that the dislocation loop densities were  $\sim 2.9 \times 10^{22} \text{m}^{-3}$  for the neutron irradiated material and only  $\sim 1.4 \times 10^{22} \text{m}^{-3}$  for the ion irradiated material. Cr segregation to loops was only found for the neutron-irradiated material. The nanoindentation hardness increase due to neutron irradiation was 3 GPa, and that due to ion irradiation 1 GPa. The differences between the effects of the two irradiation types are discussed, taking into account inconsistencies in damage calculations, and the differences in PKA spectra, dose rate and transmutation products for the two irradiation types.

# 1 Introduction

The use of heavy ion implantation for the simulation of neutron irradiation under reactor conditions is common practice, due to the short time scales to reach relatively high damage levels and the absence of induced radioactivity; the latter avoids costly requirements for additional handling precautions and the use of hot cell facilities. However, there are issues with the correlation of the effects on microstructure and mechanical behaviour between ion implantation and neutron irradiation (usually from a fission reactor). Additionally, the use of either type of radiation for investigating likely response of materials within a fusion environment has limitations; for example, the deuterium-tritium fusion neutron energy spectrum includes a peak in neutron flux at 14.1 MeV, compared to lower energies in typical fission spectra, with few neutrons of energy higher than 5 MeV [1]. The fast fusion neutrons also produce significant levels of solid and gaseous transmutation products in structural materials such as steels, tungsten and SiC, which can be difficult to simulate, even with dual- and triple-beam ion irradiation facilities. Therefore it is recognised that all sources of irradiation have specific characteristic effects on materials and the limitations of each type of irradiation must be accounted for when interpreting data.

Mechanical testing of irradiated materials may be constrained by volume limitations: either by laboratory limits in handling radioactive material, or by the limited depth of the micron-scale damage layers typically produced by heavy ion implantation. The challenges in measuring mechanical properties of ion irradiated materials are discussed further in refs. [43, 44]. For the fusion materials community, small irradiation volumes are common amongst all concepts for Early Neutron Source accelerator-driven high-energy neutron sources proposed in the EU 'roadmap to the realisation of fusion energy' [2]. It has long been established that the mechanical response of a material is not independent of specimen size, particularly at

small sizes [3]; therefore, the reduction of test specimen dimensions required to utilise these radiation sources presents a significant risk to the validity of data available.

This paper reports on a systematic study conducted on the effects of ion and neutron irradiation on the small-scale mechanical properties a model Fe 6%Cr alloy. The larger volume of radiation damage available in the neutron-irradiated material enabled the manufacture of micro-cantilever specimens with a wide range of sizes, providing an opportunity to investigate the effect of radiation damage on the mechanisms controlling the commonly observed size effect on measured strength. Samples were taken from a single batch of Fe 6%Cr alloy, irradiated with comparable doses and irradiation temperature, and tested by using identical nanoindentation and micro-cantilever methods.

## 2 Experimental Details

### 2.1 Material: Fe 6%Cr

A detailed description of the alloy manufacture and characterisation of the microstructure is given by Gelles [4]. A one hundred pound (~45 kg) heat of the Fe 6%Cr alloy was melted at the Paul D. Merica Research Laboratory in New York. Compositions provided by the manufacturer and chemical analysis performed by Lukens Steel Company (Pennsylvania) are given in *table 1*. The alloy was provided in the form of a 10mm diameter extruded bar, which was then rolled to approximately 3mm thickness.

The alloy was annealed under an argon atmosphere at 950 °C for 15 minutes followed by air cooling, then tempered at 750 °C, again followed by air cooling. This produced the microstructure shown in *figure 1*.

For the un-irradiated and ion irradiated material, sample polishing included a series of lapping stages using SiC abrasive papers from FEPA P120 to P4000 grades followed by a chemo-mechanical polish using a colloidal silica suspension (0.05  $\mu\text{m}$ ). The neutron-irradiated specimen was prepared by Idaho National Laboratory (INL) staff after irradiation. In order to reduce total activity, a 250  $\mu\text{m}$  thick, 2.3 mm diameter disc was punched from a larger sheet. The sample was ground with a series of abrasive papers to a final stage using FEPA P1200, polished using 3  $\mu\text{m}$  and 1  $\mu\text{m}$  diamond suspensions, followed by a chemo-mechanical polish using a colloidal silica suspension (0.05  $\mu\text{m}$ ).

## **2.2 Neutron Irradiation**

A sample was irradiated in capsule 6A in the ATR1 materials test reactor in INL at a controlled temperature of  $288\text{ }^{\circ}\text{C} \pm 12\text{ }^{\circ}\text{C}$ . The duration of the irradiation cycle was approximately 9 weeks and had a target total dose of 1.7 dpa. The geometry of the sample used in this study is a 2 mm diameter disc  $\sim 200\text{ }\mu\text{m}$  thick, corresponding to a volume of  $\sim 0.6\text{ mm}^3$ .

The total activity of the sample was measured at 199 MBq; *Table 2* shows the activity measurements for the sample. Dose rate measurements were 0.15 mSv/hr gamma (15 mrem/hr) and 0.9 mSv/hr beta (90 mrem/hr) on contact and 0.01 mSv/hr gamma (1 mrem/hr) at 30 cm.

## **2.3 Ion Irradiation**

Ion implantations using iron ions were conducted at the 3 MV-Tandetrion accelerator at Helmholtz-Zentrum Dresden-Rossendorf. The implantation was designed with multiple ion charges, energies and beam currents in an attempt to maintain a constant level of damage

and dose rate with depth into the sample. The beam was scanned at ~1 kHz over the sample during irradiation. The beam conditions used are shown in *table 3*.

The implantation temperature was measured and controlled at 288 °C by a thermocouple mechanically clamped adjacent to the samples on the base plate. The beam conditions were designed according to SRIM detailed calculation with full damage cascades [5] using a displacement energy for iron of 40 eV [6] and produced an average damage of 1.7 dpa in a layer 2 µm in depth from the sample surface as shown in *figure 2a*. Beam currents were set during implantation to give a consistent peak dose rate of  $5 \times 10^{-5}$  dpa/s for all energies (*figure 2b*).

## **2.4 Nanoindentation and Micro-Cantilever Testing**

Nanoindentation was conducted with an MTS NANO Indenter XP (MTS NANO Oak Ridge Tennessee, USA) with a single Berkovich tip; the tip shape was calibrated before each test series. The “continuous stiffness measurement” (CSM) indentation and analysis method [7] was used to make at least 16 indents with a depth of 1000 nm in each sample, in arrays with a indent-to-indent spacing of 40 µm. The amplitude and frequency of the CSM technique was 2 nm and 45 Hz respectively. Due to the small grain size of the samples, data from each indent series, averaged across all indents, includes the response of several grains.

Micro-cantilevers were manufactured by Focused Ion Beam (FIB) milling in the un-irradiated and ion irradiated material using a Zeiss Auriga FIB/SEM dual beam system in the Department of Materials, Oxford University. Micro-cantilevers were manufactured in the neutron irradiated material using the ‘hot’ FEI Quanta dual beam microscope at the Center for Advanced Energy Studies in Idaho Falls (USA). The following test specimens were produced:

- i. Neutron irradiated sample - 66 cantilevers with cross-sectional heights from 0.82 to 7.30  $\mu\text{m}$  (*figure 3*).
- ii. Ion irradiated sample - 30 cantilevers with cross-sectional heights from 0.36 to 2.3  $\mu\text{m}$
- iii. Un-irradiated sample - 32 cantilevers with cross-sectional heights from 0.53 to 5.11  $\mu\text{m}$

The cantilever beams were FIB milled by using various beam currents depending on the beam size and were finished with lower polishing currents to achieve a geometry with sharp edges. The All beams were measured by stereo-imaging techniques using the principles described in *ref.* [8]. Tests were conducted using the Nano-XP nanoindenter by bending the beams to a final maximum peak strain (at the lower surface at the beam root),  $\varepsilon_{max}$ , of  $\sim 0.05$  and a target strain rate at the beam root surface of  $2 \times 10^{-4} \text{ s}^{-1}$ ; for the varying beam sizes, this required controlled displacement rates from 1.4 to 30  $\text{nm s}^{-1}$ . The stress-strain response from each test was calculated from the load-displacement data,  $P-\delta$ , measured with the nanoindenter. Maximum stress for the triangular beams were calculated by integrating the second moment of area for a triangular beam,  $= \frac{wh^3}{36}$ , with the equation for stress using simple beam theory,  $\sigma = \frac{My}{I}$ , where  $y = \frac{2h}{3}$ :

$$\sigma_{max} = \frac{24Pl}{wh^2} \quad (\text{eq. 1})$$

Similarly maximum strain was calculated by using eq.1 and  $\varepsilon = \frac{\sigma}{E}$  from Hooke's Law, and the equation for maximum deflection of a cantilever beam loaded at the free end  $\delta = \frac{Pl^3}{3EI}$  from simple beam theory:

$$\varepsilon_{max} = \frac{2\delta h}{l^2} \quad (\text{eq. 2})$$

where  $l$  is the distance between the beam's fixed end and the point of loading, and  $w$  is the beam width. The elastic modulus was calculated from the initial linear gradient of the stress-strain curve, and the proof stress was calculated as the stress at the point of interception between the stress-strain curve and a line with a gradient equal to the elastic modulus and x-intercept at 0.2% strain.

Errors were calculated by summing measuring and calculating all errors for elastic modulus and stress equations in quadrature:

$$\partial E = \sqrt{\left(\frac{E}{P}\right)^2 \partial P^2 + \left(\frac{3E}{l}\right)^2 \partial l^2 + \left(\frac{-E}{\delta}\right)^2 \partial \delta^2 + \left(\frac{-E}{w}\right)^2 \partial w^2 + \left(\frac{-3E}{h}\right)^2 \partial h^2} \quad (\text{eq. 3})$$

$$\partial \sigma = \sqrt{\left(\frac{\sigma}{P}\right)^2 \partial P^2 + \left(\frac{\sigma}{l}\right)^2 \partial l^2 + \left(\frac{-\sigma}{w}\right)^2 \partial w^2 + \left(\frac{-2\sigma}{h}\right)^2 \partial h^2} \quad (\text{eq. 4})$$

Each micro-cantilever test was modelled using Finite Element Analysis (FEA) to fit the simulation load-displacement curves to the experimental data by changing the modelled material's isotropic stress-strain properties, via a process of progressive convergent approximation. The continuum isotropic plasticity model used in FEA could not represent the stochastic nature of plasticity at the micron scale, hence the aim was to fit the model to the averaged experimental curve. A series of MATLAB functions was written to automate several tens of FEA simulations required for the fitting of data within a specified accuracy, and the final model isotropic stress-strain properties were recorded.

The radiation damage microstructures of these irradiated alloys have been characterised by Transmission Electron Microscopy (ion irradiated specimen) and Atom Probe Tomography (neutron and ion irradiated specimens). Results have been reported in detail elsewhere [9, 10], but are summarised in this paper when discussing likely hardening mechanisms.



## 3 Results

### 3.1 Nanoindentation

Nanoindentation data for elastic modulus versus indentation depth are shown in *figure 4a*. At shallow indentation depths the measured elastic moduli for ion and neutron irradiated materials are similar and are higher than for the un-irradiated material. As the indentation depth increases, the measured elastic modulus for the ion-irradiated material tends towards the values for the un-irradiated material, which correlates with an increasing influence on the measured modulus from the un-irradiated bulk substrate material below the ion-irradiated layer.

The modulus measured by the nanoindenter may be affected by errors in the tip to surface contact area calculated from the indenter displacement,  $h_c$ , and tip area function,  $f(h_c)$ , resulting from plastic pile-up of material surrounding the indents. Post-indentation contact area measurements of all indent impressions in the un-irradiated and neutron irradiated material were conducted by Scanning Electron Microscopy (SEM) imaging (*figure 5*). This was done by measurement of the projected contact area, which is clearly visible by a sharp change in surface gradient (edge) of the indent pit using a similar method to that of Tsui et al. [45]. This area measurement is then used to calculate area-corrected values of hardness and elastic modulus using the same equations as reported in ref. [7]. Elastic modulus was then recalculated for the maximum indentation depth of 1000 nm using the measured post-indentation contact area for each indent; the average values with standard deviation are shown in *figure 4a* ("Area Correction" points). The use of actual contact area gives derived modulus values lower than those calculated from tip area functions; however modulus of

the neutron-irradiated material is still calculated to be ~15% greater than that of the unirradiated material.

*Figure 4b* shows average values for hardness versus indentation depth, and hardness values at maximum indentation depth corrected for post-indentation contact area measurement. Irradiation hardening is clearly evident in both irradiated alloys; however the hardening in the neutron-irradiated material is more than double that in the ion-irradiated material. Similar to the elastic modulus measurements, hardness in the ion-irradiated material tends towards the un-irradiated hardness as the indentation depth increases. Larger pile-up surrounding the indenter tip in the neutron-irradiated material results in a slight over estimation of irradiation hardening in calculations based on the tip area function; however pile-up in the ion-irradiated material may also overestimate the irradiation hardening.

Typical SEM images of indent impressions in the un-irradiated and neutron irradiated material are shown in *figure 5*. Plastically deformed material forming the pile-up lobes showed diffuse slip lines in the un-irradiated material and highly localised slip steps in the neutron-irradiated material. In both cases, slip lines were wavy and curved, rather than linear, indicating extensive cross slip of dislocations between available slip planes.

### **3.2 Micro-cantilever Testing**

Typical stress-strain curves for micro-cantilever tests of various sizes are shown in *figure 6*. For the un-irradiated material, as plastic deformation progresses, large load drops are visible, which tend to increase in magnitude as the beam sizes increase. Such load drops were not observed in either the ion- or neutron- irradiated alloys, where plastic deformation produced smooth variations in load. Very little work hardening was observed in the un-

irradiated and ion-irradiated material. In comparison, the neutron-irradiated material clearly exhibits work hardening.

The elastic modulus measurements with error bars calculated using the simple beam theory methods described in *section 2* are plotted in *figure 7* for all cantilever tests. A large scatter in the modulus between ~150 and 350 GPa was observed in the smallest cantilevers, which may be partially attributed to variations in crystal orientation across each test (the elastic modulus of pure Fe varies from ~125 GPa along the <100> axis to 275 GPa along the <111> axis [11]). As the beam size increases, more grains contribute to the elastic modulus measurements and the scatter decreases; these values should tend towards approximately 210 GPa, the macroscopic polycrystalline value [12]. The values of elastic modulus measured in the largest beams appear to be slightly lower than this value; this may be due to lower stiffness measurements caused by the deformation of material at the base of the beam and surrounding the indenter tip; this is not taken into account in the simple beam model, which assumes an purely elastic cantilever, rigidly fixed at one end.

The proof stresses calculated at 0.2% strain offset versus the beam height are plotted in *figure 8*. All three materials exhibit an increase in the measured proof stress as the cantilever size decreases. In the neutron-irradiated material, proof stress values above those for the unirradiated material are clearly evident across the entire range of beam sizes. In the ion-irradiated material the proof stress values for beams with  $h < 1 \mu\text{m}$  are not separable from those for unirradiated beams. For each material, it was found that the proof stress,  $\sigma_{proof}$ , could be fitted closely to a function of the form:

$$\sigma_{proof} = A_0 h^{-1} + A_1 \quad (\text{eq. 5})$$

where  $h$  is the beam height and  $A_1$  is the asymptotic value of proof stress ( $\sigma_{proof}$  at  $h = \infty$ ). The fitted curves are shown in *figure 8*. The values for  $A_0$  and  $A_1$  are given in *table 4* with the correlation coefficient  $R$ ; these values are discussed further in *section 4.3*.

Typical SEM images of the plastically deformed surfaces at the beam base are shown in *figure 9*. Slip steps are visible in the larger cantilever beams, but no slip steps were observable in the smallest beams. Large beams in the un-irradiated material exhibited only a few large slip steps in the deformed region. Slip steps in both types of irradiated material are more numerous and are well-separated, suggesting plasticity progresses inhomogeneously within localised slip planes.

### 3.3 Radiation damage microstructures

The radiation damage defect types, sizes and densities found in previous studies of these irradiated materials [9,10] are summarised in *Table 5*. The main points are that:

- 1) Dislocation loops are of  $\frac{1}{2}\langle 111 \rangle \{111\}$  type for both irradiation methods.
- 2) For the ion irradiated material, there is good agreement between the TEM and the APT measurements for the number density of loops:  $1.3$  to  $1.4 \times 10^{22} \text{ m}^{-3}$ .
- 3) The loop number density in the neutron irradiated material ( $2.9 \times 10^{22} \text{ m}^{-3}$ ) is roughly double that in the ion-irradiated material.
- 4) APT finds somewhat larger loops than TEM. Considering both techniques, typical loop diameters are  $\sim 6$ - $9$  nm in ion-irradiated material, and bimodal in the neutron irradiated materials ( $\sim 9$  nm and  $\sim 18$  nm).
- 5) Chromium segregation to the loops is found only in the neutron irradiated sample, but Si segregates (more weakly than chromium) to the loops for both irradiation types.

## 4 Discussion

The experiments reported in this paper were conducted with two objectives. The first objective was to assess the validation of ion implantation as an analogue for neutron irradiation, by means of a direct comparison. The second objective was to investigate the influence of irradiation hardening on the intrinsic size effects on sample strength, by conducting micro-mechanical testing with test specimens of various sizes. The implications of the results on both objectives are discussed below.

### 4.1 Hardening effects of radiation damage

The irradiation hardening due to damage from neutrons or ions can be considered in terms of interactions between mobile dislocations and the observed dislocation loops (and their associated solute clusters). If it is assumed that the loops act as local obstacles to dislocation motion, their effect on increasing the shear flow stress on the material (by  $\Delta\tau_y$ ) can be modelled as either:

$$\Delta\tau_y = \frac{Gb}{\lambda} [\cos(\phi_c)]^{\frac{2}{3}} \quad (eq. 8)$$

Or

$$\Delta\tau_y = \frac{Gb}{\lambda} \cos(\phi_c), \quad (eq. 9)$$

where  $G$  is the material's shear modulus (82 GPa for iron),  $b$  is the length of the Burgers vector (0.248 nm),  $\lambda$  is the inter-obstacle spacing and  $2\phi_c$  is the critical angle subtended by the two arms of the dislocation as it breaks away from an obstacle. The parameter  $\phi_c$  characterises the obstacle strength, with low values implying a strong obstacle; at one limit, when  $\phi_c = 0$ , the obstacle is impenetrable, and the dislocation will pass the obstacle by the

Orowan bowing process, at the other limit, when  $\phi_c = 90^\circ$ , the dislocation passes the obstacle without hindrance. Equation (8), the “Friedel relation”, applies when obstacles are weak ( $\phi_c > \sim 50^\circ$ ), with the radius of dislocation line curvature under the applied stress being much greater than the typical inter-obstacle spacing [33, 34]; equation (9) applies when obstacles are strong ( $\phi_c < \sim 50^\circ$ ), with the radius of dislocation line curvature being of the same order as the typical inter-obstacle spacing [33].

The inter-obstacle spacing,  $\lambda$ , is determined as:

$$\lambda = [\rho \cdot d]^{-\frac{1}{2}} - d \quad (\text{eq. 10})$$

where  $\rho$  is the number of obstacles, of diameter  $d$ , per unit volume.

To obtain first-approximation values for  $\phi_c$  for the obstacles in the ion-irradiated and neutron irradiated materials, we use the nanoindentation data rather than the microcantilever data, as being less subject to scaling effects. Figure 4b indicates that the hardness increase due to ion-irradiation is  $\sim 1$  GPa and that due to neutron irradiation is  $\sim 3$  GPa; we take hardness as being  $\sim 3\times$  (tensile) yield stress [41], and shear flow stress as being  $\frac{1}{2}$  the yield stress (according to a maximum possible Schmid factor of 0.5 for a single crystal). Table 5, in the bottom 5 rows, shows results of these calculations (note that the data for defect sizes used for the ion-irradiated material were the mean value of those derived from TEM and APT data; for the neutron irradiated data, the mean of the values derived for the two loop sizes). These rather crude calculations indicate that

- 1) the obstacle spacing is significantly less in the neutron-irradiated material than in the ion-irradiated material (even given the uncertainties in dealing with the bimodal size distribution in the neutron-irradiated material),

- 2) in both cases the loops are relatively strong obstacles, and are therefore best dealt with by equation (9),
- 3) the obstacle strength in the neutron irradiated material is significantly higher than in the ion-irradiated material.

The greater hardness increase due to neutron irradiation, compared with ion irradiation, thus results from both an increased dislocation loop density, and from the loops having greater obstacle strength to gliding dislocations. This greater obstacle strength in the neutron irradiated material is likely to be related to the higher level of segregation of chromium (and possibly silicon) to the dislocation loops. Greater obstacle strength in the neutron irradiated alloy is also consistent with the observation of work hardening in micro-cantilever tests, where it is possible that additional hardening features such as Orowan loops are produced when glissile dislocations overcome strong obstacles.

## **4.2 Size Effects in Irradiated Materials**

The observed increase in mechanical strength of a material with decrease in test specimen size is a well-known phenomenon. The first observations of size dependence in tensile strength were made by Brenner in 1956 by tensile testing whiskers of iron, copper and silver from 1.2  $\mu\text{m}$  to 15  $\mu\text{m}$  in diameter [3]. There have been several attempts to characterise the underlying mechanisms which produce this effect, yet at present there is no clear explanation which can account for all of the various observations throughout the literature.

The mechanisms identified which result in size effects are:

- i. Strain gradient plasticity theory (beam bending and indentation)
- ii. Dislocation starvation
- iii. Dislocation truncation

- iv. Dislocation pile-up at the beam neutral axis (beam bending only)

A variation of hardness with indentation depth is commonly observed in many materials and provides a method to measure the size dependence of strength in a single test. Nix and Gao [35] developed a law for strain gradient plasticity which suggests that the density of geometrically necessary dislocations (GNDs) required to support the shape of the indent impression is responsible for the indentation size effect (ISE). Assuming a simplified model comprising of a rigid conical indenter and deformation accommodated by circular GNDs in a hemispherical volume beneath the indenter tip, the density of GNDs is defined as [35]:

$$\rho_{GND} = \frac{3}{2bh} \tan^2 \theta \quad (\text{eq. 11})$$

where  $\theta$  is the centreline-to-face angle of the indenter tip,  $b$  is the Burgers vector and  $h$  is the indentation depth. Thus, as the indenter is driven into the sample surface,  $\rho_{GND}$ , and thereby the contribution to hardness due to work-hardening effects, decreases with indentation depth.

This theory does not apply to the strong size effect observed in micro-pillar tests [36], where there are no strain gradients produced from uniaxial loading. It has been proposed that the lack of dislocation multiplication events during the deformation of such small volumes may lead to a lack of available dislocations, termed dislocation starvation, and requires the nucleation of dislocations at a higher stress [37]. Similarly, dislocation sources require a characteristic volume to operate. The fabrication of test specimens may create surfaces which reduce the length of available dislocation segments and limit the volume available for source operation; these shorter segments and sources may require higher stresses to operate, known as truncation hardening [38].



The theories of source starvation and truncation suggest that plastic deformation is increasingly controlled by the activation characteristics of dislocation sources as the size of the test volume decreases. In the present work, there are two observations which indicate that the activation of dislocation sources influence plasticity in the tests. Firstly, discrete pop-in events in the load-displacement behaviour were observed during nanoindentation at small depths in several tests on all samples. This represents the transformation from elastic to fully plastic deformation by the activation of dislocation sources. Secondly, as commonly observed in other micro-mechanical tests [39], plasticity in the micro-cantilever tests shown in *figure 6* progressed in a stochastic nature exhibiting several drops in load during mechanical testing. These load drops are likely to be related to the activation of individual sources as the deformation progresses.

As shown in *figure 6a*, the magnitude of the load drops increases with increasing beam size in the un-irradiated material. The magnitude of the load drop may be proportional to the strain accommodated once a dislocation source has been activated; it is likely that this strain is controlled by the number of dislocations which can be emitted before stresses produced by pile-up at the neutral axis cause the source to shut down. Hence, the increase in magnitude of the load drops with increasing beam size may relate to the longer distance dislocations glide on larger slip planes, which accommodate a greater number of dislocations emitted from a single source. This observation is supported by the appearance of visible slip steps at the surface only in the larger plastically deformed beams in *figure 9*, where each slip plane can accommodate a greater number of dislocations.

Load drops in cantilever tests indicate that the stress to activate dislocation sources dominates the observed strength of the material, resulting in no difference in the yield stress between the un-irradiated and ion-irradiated material for beams  $<1\ \mu\text{m}$  depth. A similar

observation was made in the investigation conducted by Kiener et al. [40], where no irradiation hardening in proton irradiated Cu was measured in micro-pillar tests below a diameter of 400nm. However, even though the measured yield stress does not change with irradiation, strain localisation characteristics may differ; Kiener et al. identified that glissile dislocations partially or fully remove the irradiation-induced defects and that plastic deformation developed by localised slip within defect-free channels. The highly localised slip steps observed in the irradiated material around indents (*figure 5*) and at the deformed surfaces of micro-cantilevers (*figure 9*) suggests that the material investigated here deforms in a similar manner. This type of plastic deformation has been characterised for an ion-irradiated Fe 12%Cr alloy [20] and is caused by the annihilation of irradiation-induced defects by glissile dislocations. In the presence of high stresses produced to overcome size effect mechanisms, the defects may be annihilated without additional stress and plastic deformation progresses at the same stress as the un-irradiated material.

When the size of the test specimen increases above a critical size ( $\sim 1\text{ }\mu\text{m}$  in the present case), the stress determined by the size effect mechanisms is lower than that determined by the irradiation-induced defects and the response of the ion-irradiated material deviates from that of the un-irradiated material. In Kiener's study [40], this critical size was found to be a pillar diameter of 400nm, above which the yield stress of the irradiated Cu was apparently independent of size. This is clearly not observed in the tests reported here where the yield stress of the irradiated material continues to decrease as the beam depth increases.

Unlike the behaviour of ion-irradiated material, irradiation hardening measured for the neutron irradiated material was not completely obscured in the smallest beams. This suggests that the interaction between glissile dislocations and irradiation induced defects is different for the defects produced by ion-irradiation and those produced by neutron-

irradiation. As suggested in *section 4.1*, the neutron-irradiated material is likely to exhibit Cr enrichment associated with radiation damage dislocation loops. Unlike the “clean” dislocation loops, areas of Cr enrichment cannot annihilate by reaction with a glissile dislocation, and thus will contribute to the stress required for plastic deformation in addition to the mechanisms controlling the size effect. Furthermore, the increased work hardening behaviour observed in the neutron-irradiated material indicates the resistance to annihilation of Cr enriched regions. .

### **4.3 Comparison with Macro-Scale Properties**

The Fe 6%Cr material studied here was also investigated by Vickers micro-hardness testing. A LECO LM247 AT instrument was operated with a load of 500 g, to produce indents into both the un-irradiated and neutron irradiated material. Values of hardness were 117.2 Hv (+/- 2.7) for the un-irradiated material and 232.9 Hv (+/- 5.8) for the neutron-irradiated material. Dividing these values by 3 (see ref. [41]) provides an estimate of the macro scale yield stress; this produces a yield stress of 383 MPa for the un-irradiated material and 762 MPa for the neutron-irradiated material. Using the same technique on the nanoindentation measured hardness at the maximum displacement of 1000 nm produces hardness values of ~500 MPa for the un-irradiated material and ~1000 MPa for the neutron irradiated material, suggesting that the results are subject to indentation size effect.

The micro-cantilever data described in *section 3.2* may provide a means for extrapolation to macro scale properties. The observation that the proof stress is strongly proportional to  $h^{-1}$  was also made by Motz et al. [39] for micro-cantilever tests in a copper single crystal. Motz provided an analytical model which accounts for the increase in flow stress produced by the pile-up of dislocations at the neutral axis. This contribution,  $\sigma_{PU}$ , is given by:

$$\sigma_{PU} = \frac{\alpha G}{b} \frac{\omega^2}{x^2} h \lambda^2 \quad (\text{eq. 12})$$

where  $\alpha$  is a constant (0 to 1),  $G$  is the shear modulus (84 GPa for iron),  $b$  is the Burgers vector (248 pm for iron),  $\omega$  is the beam bending angle,  $x$  is the size of the plastically deformed region,  $h$  is the beam height and  $\lambda$  is the dislocation source spacing. The assumption that the size of the plastically deformed region can be approximated as the beam thickness<sup>1</sup> ( $x = h$ ) gives [39]:

$$\sigma_{PU} = \frac{\alpha G}{b} \frac{\omega^2}{h} \lambda^2 \quad (\text{eq. 13})$$

According to *the equations in section 3.2*, values of  $A_0$  may be described by:

$$A_0 = \frac{\alpha G}{b} \omega^2 \lambda^2 \quad (\text{eq. 14})$$

Using the fitted values for  $A_0$  in *table 4* produces an average dislocation source spacing from ~20 nm to ~200 nm for the three materials at values of  $\alpha$  from 0.1 to 0.9. This range corresponds well with the distribution of slip steps in the deformed beams shown in *figure 9*.

The values for  $A_1$  in *table 4* represents the asymptotic values of proof stress ( $\sigma_{proof}$  at  $h = \infty$ ) of 477 MPa for the un-irradiated and 1290 MPa for the neutron irradiated material, which is similar to the yield stress calculated from nanoindentation hardness as described above. These values are larger than the values of yield stress calculated from the Vickers hardness data and indicate that additional size effect mechanisms such as source

---

<sup>1</sup> A large extent of the plastically deformed region is more likely to be confined within the bottom half of the beam, however the entire beam thickness is assumed here for consistency with the method developed by Motz et al. [39]

starvation/truncation may also contribute to the response of the material. This suggests that the extrapolation of yield stress to macro scale properties requires a more complex model of the mechanisms which contribute to the size effect or a larger range of test sizes.

#### **4.4 Comparison of Ion and Neutron Irradiation**

The production and evolution of radiation damage in a given material depends on several parameters including the type and energy of the irradiating particle, the fluence / dose (number of displacements, dpa), the irradiation temperature and flux/dose rate (damage rate, dpa/s) [13]. The current experiment produced neutron and ion irradiated materials with planned dose of 1.7dpa and irradiation temperature of 288 °C, yet the nanoindentation measurements presented in *figure 4b* and micro-cantilever results in *figure 8* show clear differences between hardening produced by irradiation with ions and that with neutrons. These differences might be caused by inconsistencies in damage calculations, the different PKA energy spectra between the two irradiation types, the presence of transmutation He and H in neutron-irradiated materials only, or by differences in damage types and densities produced by irradiation at different dose rates.

##### **4.4.1 Damage Calculations – Neutron Irradiation**

Three different methods were used to calculate the level of radiation damage in the neutron irradiated alloy:

**Method 1:** The dose was calculated using the damage rate equation [14] and post irradiation fluence measurements as a function of neutron energy,  $\phi(E_i)$ , and the energy-dependent displacement cross-section,  $\sigma_D(E_i)$ , for the neutron irradiated material produced at INL. :

$$R_d = N \int_{\hat{E}}^{\hat{E}} \phi(E_i) \sigma_D(E_i) dE_i \quad (\text{eq. 6})$$

This produced a dose value of **1.83dpa**.

**Method 2:** The PKA energy (recoil) spectra for the neutron irradiated material were calculated using the NJOY-2012 code [15] (to produce recoil probability matrices,  $\sigma(E_i, T)$  defined in *equation 2.3*) and SPECTER (to collapse these matrices with the ATR1 spectrum). The PKA energy spectra for the dominant reactions during irradiation are plotted in *figure 10*. The results from a FISPACT-II inventory simulation [16] produced a value for total damage of **1.63dpa**.

**Method 3:** The damage energy,  $T$ , as a function of PKA energy,  $E_i$ , in iron was calculated using the data and relationships produced by Dierckx [17]; this is shown in *figure 11*. The damage energy was used with the modified Kinchin and Pease NRT formula [18]:

$$dpa_{NRT} = \frac{0.8T}{2Ed} \quad (\text{eq. 7})$$

This method produced a value for total damage of **1.72dpa**.

All three values are thus reasonably consistent at 1.7 dpa, +/-0.1 dpa.

#### **4.4.2 Damage Calculations – Ion Irradiation**

For the configuration of the ion implantations, doses were calculated by using the ‘Detailed Calculation with Full Damage Cascades’ model in SRIM as shown in *figure 2*, producing a uniform damage layer with an average damage of 1.7 dpa over 2 $\mu$ m. However, the application of method 3, by using the same damage energy function produced by Dierckx [17] and NRT formula produces a value of ~0.5 dpa. This discrepancy is caused by inconsistencies in the SRIM codes, as has been confirmed by Stoller et al. [19]. As recommended by Stoller, the ‘Quick Calculation of Damage’ (Kinchin-Pease) model in SRIM

was used to calculate the actual ion implantation dose. The damage energy,  $T$ , was calculated by:

$$T = E_i^0 - E_i^I - E_T^I = E_i^P + E_i^B + E_T^P + E_T^B, \quad (\text{eq. 8})$$

where the energy of the incident ion is distributed into electronic stopping (superscript  $I$ ), lattice binding energy (superscript  $B$ ) and lattice phonons (superscript  $P$ ), from the incident ions (subscript  $i$ ) or the target atoms (subscript  $t$ ). In order to remain consistent with the NRT model used for the neutron irradiation, the lattice binding energy was set to zero and the number of phonons/Å-ion was used to give  $T$ . This produced an average damage with depth of 0.82 dpa and is shown with the original target of 1.7 dpa in *figure 12*.

Thus it is likely that the neutron irradiated alloy was physically subjected to more displacement damage, which may have contributed to the higher number of defects and segregation of Cr observed for this material. However, several ion implantation studies of a similar alloys have identified that irradiation hardening saturates at a doses of 1-2 dpa (calculated by using the ‘Detailed Calculation with full Damage Cascades’ model) [20,21]. Thus, a variation in dose alone is unlikely to explain the large difference in hardening between the ion and neutron irradiated materials.

#### **4.4.3 The Effect of PKA Energy Spectra**

Fission neutrons produce PKA energies of up to 200 keV [17] and have an energy spectrum which includes a tail of lower energies. In comparison, in ion implantation experiments each incident ion simulates a PKA with an energy equal to that of the beam energy (up to 9 MeV in the current experiment) [22,23]. Using recoil spectra for  $^{56}\text{Fe}$  and calculations of displacements from method 3 above, the damage as a function of PKA energy produced by the ion and neutron irradiations is shown in *figure 13*.

The difference in the total number of displacements produced by each incident particle should be accounted for in the damage calculations for each irradiation; thus, areas beneath the curves for ions and neutrons in *figure 13* should be equal to the total dose calculated for each method. However, the types of primary defects produced by an incident ion or neutron may differ depending on the PKA energy. There is agreement amongst several authors [17, 24-26] that above a threshold damage energy of approximately 5 to 10 KeV, the production of primary defects in a material is independent of damage energy. The threshold energy represents the transition from the production of Frenkel pairs at the lowest PKA energies to larger cascades and sub-cascade formation at higher PKA energies. Above this threshold energy, formations of separate sub-cascades produce the same primary defect types and the numbers of these defects remain a constant function of the energy (30% of the NRT value [26]). On the other hand, recent MD simulations [27] identified that cascades were in the form of a continuous distribution of damage and that the primary defect morphology continues to change as a function of energy up to 0.5 MeV.

For the neutron irradiation, the majority of the damage was produced by PKA energies from ~60 to 275 keV with a peak at 158 keV. In contrast, PKA energies produced during the ion implantation were 0.5 to 9 MeV. This suggests that the cascade damage morphology produced by the fission neutrons may be significantly different to that produced by ion implantation. This is likely to influence the fraction of freely migrating defects in both ion and neutron irradiations [28, 29]; that is, the fraction of isolated point defects or defects within small clusters which are mobile. The fraction of freely migrating defects produced within an irradiated material will directly influence diffusion mediated processes such as creep, swelling and radiation induced segregation (RIS). In the current experiment, differences in the PKA energies between the ion and neutron irradiated sample may have



contributed to the observed RIS of Cr in the neutron irradiated sample. The influence of freely migrating defects is also determined whether on average they recombine and annihilate, or agglomerate to form dislocation loops or voids, or migrate to sinks such as grain boundaries etc. This is directly influenced by dose rate as described below.

#### ***4.4.4 The Effect of Dose Rate***

The dose rate of the ion-implantation was approximately 500 times higher than for the neutron irradiation. The rate of interaction between cascade defects is dependent on defect mobility and is proportional to the square of the defect density. The lower dose rate neutron irradiation results in a lower defect density in a given volume per unit time; this may result in a lower number of defect interactions and an increase in the length of defect migration paths compared to higher dose rates. Increasing rates of irradiation creep and swelling with decreasing dose rate have been shown for austenitic steels [30, 31]. More recently an increase in irradiation hardening at lower dose rates was shown in ion-irradiated Fe-Cr alloys of similar composition [32]; here it was shown that heightened Cr segregation was the cause of additional hardening in the alloy irradiated with the lowest dose rate. The observation of Cr segregation described in section 3.3 and table 5, is comparable to that reported in ref. [32] and thus is likely to have been the primary cause of higher irradiation hardening produced by neutron irradiation compared to ion irradiation.

As discussed, the variation in the effects of irradiation with different dose rates has been identified elsewhere. Methods to overcome variation in dose rate have been proposed, such as the use of a temperature shift to manipulate defect mobility and accommodate a different dose rate [42]. However, radiation produces several types of defect all with a characteristic mobility which cannot be accommodated by a single temperature shift. A

temperature shift may therefore not facilitate the complete comparison of irradiations conducted at different rates accurately.

#### **4.4.5 Transmutation He and H**

In addition, the FISPACT-II inventory simulation indicated that approximately 10 appm He and 6.5 appm H was produced in the alloy during neutron irradiation. This may have also contributed to the increase in irradiation hardening.

## **5 Summary**

- i. Fe 6%Cr irradiated to a nominal dose of 1.7 dpa at 288 °C exhibited significantly different irradiation hardening depending on whether the irradiation was by ions or by neutrons.
  - a. Nanoindentation results showed that irradiation hardening in the neutron-irradiated material was ~3 GPa, whilst it was ~1 GPa in the ion-irradiated material.
  - b. Unlike the un-irradiated and ion-irradiated material, the neutron-irradiated material exhibited some work hardening in micro-cantilever tests.
- ii. The variation of hardening may be caused by:
  - a. Inconsistencies in damage calculations between the standard NRT formula for neutron irradiations and 'detailed calculation with full damage cascades' model in TRIM for ion-irradiation. As described in *section 4.4.2*, comparison with similar work suggests that the ion implantation damage is likely to be at or near saturation.

- b. A difference in the characteristics of the radiation damage introduced by the two radiation types has been observed; principally a higher density of dislocation loops in the neutron irradiated material ( $2.9 \times 10^{22} \text{ m}^{-3}$ ) compared to the ion irradiated material ( $1.4 \times 10^{22} \text{ m}^{-3}$ ) and a tendency for Cr clustering in the neutron irradiated material. This clustering is likely to be associated with the dislocation loops, making them stronger obstacle to dislocation motion, and more resistant to removal by the passage of mobile dislocations.
    - c. The presence of the enhanced Cr enriched regions in the neutron irradiated material may results from differences in the dose rate ( $5 \times 10^{-5} \text{ dpa/s}$  for ion-irradiation and  $\sim 3 \times 10^{-7} \text{ dpa/s}$  for neutron-irradiation) and/or PKA energy spectra (see *figure 13*).
  - iii. All materials exhibited a size effect with yield stress varying by up to 700% for beam depths from  $\sim 0.5 \text{ }\mu\text{m}$  to  $\sim 7 \text{ }\mu\text{m}$  (*figure 8*). The effect in the ion-irradiated material was such that hardening due to irradiation was obscured by size effects. In the neutron irradiated material, the stronger hardening due to irradiation was not fully obscured by size effects. These differences in strength and irradiation hardening are likely to have been caused by the different types of defect produced by the ion and neutron irradiations, in particular a stronger tendency to produce chromium enriched regions for the neutron irradiation where the dose rate is much lower than for ion irradiation.
  - iv. Attempts to extrapolate micro-cantilever results to the macro-scale in *section 4.3* appear unsuccessful. This is likely to be caused by errors in empirical relationships used for Vickers hardness data and/or multiple size effect mechanisms including

source activation and dislocation pile-up at the neutral axis, which require a more complex model.

## 6 Acknowledgements

Work on the neutron irradiated sample was supported by the National Scientific User Facility (NSUF) and the Center for Advanced Energy Studies-Microscopy and Characterization Suite (CAES-MaCS); in particular we thank Jatuporn Burns for assistance with the FIB at CAES-MaCS. The authors thank Mr J.W. Nielsen at INL for supplying post irradiation fluence measurements as a function of neutron energy,  $\phi(E_i)$ , and the energy-dependent displacement cross-section,  $\sigma_D(E_i)$ , for the neutron irradiated material. Thanks to Dr M. Gilbert at UKAEA for providing damage calculations using NJOY, SPECTER and FISPACT codes. Thanks to Mr T Milot at INL for supplying Vickers hardness data. The work reported here was partially supported by the Engineering and Physical Science Council (EPSRC) via a Programme Grant “Materials for Fusion and Fission Power”, EP/H018921. C.D. Hardie thanks EPSRC and the Culham Centre for Fusion Energy (CCFE) for funding in the form of an Industrial CASE studentship.

## References

- 1 R.E. Stoller, L.R. Greenwood, Subcascade formation in displacement cascade simulations: Implications for fusion reactor materials, *J. Nucl. Mater.* 271-272 (1999) 57-62.
- 2 F. Romanelli, P. Barabaschi, D. Borba, G. Federici, L. Horton, R. Neu, D. Stork, H. Zohm, Fusion Electricity: A roadmap to the realisation of fusion energy. EFDA Report (2013)
- 3 S.S. Brenner, Tensile strength of whiskers, *J. Appl. Phys.* 27 (1956) 1484-1491.
- 4 D.S. Gelles, Microstructural examination of neutron-irradiated simple ferritic alloys, *J. Nucl. Mater.* 108-109 (1982) 515-526.
- 5 J.F. Ziegler, M.D. Ziegler, J.P. Biersack, SRIM – The stopping and range of ions in matter (2010), *Nucl. Instrum. Methods. B268* (2010) 1818-1823.
- 6 Standard Practice for Measurement of Mechanical Properties during Charged-Particle Irradiation. ASTM International E821 - 96(2009).
- 7 W.C. Oliver, G.M. Pharr, An improved technique for determining hardness and elastic modulus using load and displacement sensing indentation experiments., *J Mater Res.* 7 (1992) 1564-1583.
- 8 G. Piazzesi, Photogrammetry with the scanning electron microscope, *J. Phys. E: Sci. Instrum.* 6 (1973) 392-396.
- 9 Y. Wu, P. Wells, G. R. Odette, T. Yamamoto, S. Roberts, C. Hardie, D. Bhattacharyya, M. Bachhav and E. A. Marquis, Microstructural characterization of a Fe+ irradiated Fe-6%Cr alloy, US Department of Energy Report on the Fusion Reactor Materials Program, 2015, DOE/ER-0313/58, pp 8-11.
- 10 M. Bachhav, L. Yao, G. R. Odette, E. A. Marquis, *J. Nucl. Mater.* 453 (2014) 334.
- 11 G.E. Dieter, *Mechanical metallurgy*, McGraw-Hill New York, 1976.
- 12 G. Speich, A. Schwoeble, W. Leslie, Elastic constants of binary iron-base alloys, *Metallurgical Transactions.* 3 (1972) 2031-2037.
- 13 C. Abromeit, Aspects of simulation of neutron damage by ion irradiation, *J. Nucl. Mater.* 216 (1994) 78-96.
- 14 G.S. Was, *Fundamentals of radiation materials science: metals and alloys*, Springer, 2007.
- 15 R. MacFarlane, D. Muir, The NJOY nuclear data processing system, Los Alamos National Laboratory LA-UR-12-27079 (2012).
- 16 J. Sublet, J. Eastwood, J. Morgan, The FISPACT-II User Manual CCFE-R(11)11 Issue 3, Tech. Rep. CCFE (2012).
- 17 R. Dierckx, The importance of the PKA-energy spectrum for radiation damage simulation, *J. Nucl. Mater.* 144 (1987) 214-227.
- 18 M.J. Norgett, M.T. Robinson, I.M. Torrens, A proposed method of calculating displacement dose rates, *Nucl. Eng. Des.* 33 (1975) 50-54.
- 19 R.E. Stoller, M.B. Toloczko, G.S. Was, A.G. Certain, S. Dwaraknath, F.A. Garner, On the use of SRIM for computing radiation damage exposure, *Nuclear instruments and methods in physics research section B: beam interactions with materials and atoms* 310 (2013): 75-80.
- 20 C.D. Hardie, S.G. Roberts, Nanoindentation of model Fe–Cr alloys with self-ion irradiation, *J. Nucl. Mater.* 433 (2013) 174-179.

- 21 C. Heintze, F. Bergner, M. Hernández-Mayoral, Ion-irradiation-induced damage in Fe–Cr alloys characterized by nanoindentation, *J. Nucl. Mater.* 417 (2011) 980-983.
- 22 S. Ishino,. Implications of fundamental radiation damage studies in the research and development of materials for a fusion reactor, *J. Nucl. Mater.* 239 (1996): 24-33.
- 23 R.S. Nelson,, D.J. Mazey, J.A. Hudson, The use of ion accelerators to simulate fast neutron-induced voidage in metals, *J. Nucl. Mater* 37.1 (1970): 1-12.
- 24 R.E. Stoller, G.R. Odette, B.D. Wirth, Primary damage formation in bcc iron, *J. Nucl. Mater.* 251 (1997) 49-60.
- 25 R. More, J. Spitznagel, Primary recoil spectra and subcascade effects in ion bombardment experiments, *Radiation Effects.* 60 (1982) 27-33.
- 26 R.E. Stoller, The role of cascade energy and temperature in primary defect formation in iron, *J. Nucl. Mater.* 276 (2000) 22-32.
- 27 E. Zarkadoula, S. Daraszewicz, D. Duffy, M. Seaton, I. Todorov, K. Nordlund, M. Dove, K. Trachenko, The nature of high-energy radiation damage in iron, *Journal of Physics: Condensed Matter.* 25 (2013) 125402.
- 28 H. Wiedersich, Effects of the primary recoil spectrum on long-range migration of defects, *Radiation effects and defects in solids.* 113 (1990) 97-107.
- 29 L. Rehn, Production of freely-migrating defects, *J. Nucl. Mater.* 174 (1990) 144-150.
- 30 J.L. Seran, J.M. Dupouy, Swelling of solution annealed 316 cladding in Rapsodie and Phenix, in: J.S.P. Brager (Ed.), *Effect of Radiation on Materials: 11th International Symposium*, ASTM, Baltimore, MD., 1982.
- 31 G.W. Lewthwaite, D. Mosedale, The effects of temperature and dose-rate variations on the creep of austenitic stainless steels in the dounreay fast reactor, *J. Nucl. Mater.* 90 (1980) 205-215.
- 32 C.D. Hardie, C.A. Williams, S. Xu, S.G. Roberts, Effects of irradiation temperature and dose rate on the mechanical properties of self-ion implanted Fe and Fe–Cr alloys, *J. Nucl. Mater.* 439 (2013) 33-40.
- 33 L.M. Brown and R.K. Ham, *Strengthening Methods in Crystals*, Applied Science Publishers, London (1971).
- 34 J.W. Martin, *Micromechanisms in particle-re-enforced alloys*, Cambridge University Press, 1980, p50.
- 35 W.D. Nix, H. Gao, Indentation size effects in crystalline materials: A law for strain gradient plasticity, *J. Mech. Phys. Solids.* 46 (1998) 411-425.
- 36 J.R. Greer, J.T.M. De Hosson, Plasticity in small-sized metallic systems: Intrinsic versus extrinsic size effect, *Progress in Materials Science.* 56 (2011) 654-724.
- 37 W.D. Nix, J.R. Greer, G. Feng, E.T. Lilleodden, Deformation at the nanometer and micrometer length scales: Effects of strain gradients and dislocation starvation, *Thin Solid Films.* 515 (2007) 3152-3157.
- 38 T.A. Parthasarathy, S.I. Rao, D.M. Dimiduk, M.D. Uchic, D.R. Trinkle, Contribution to size effect of yield strength from the stochastics of dislocation source lengths in finite samples, *Scr. Mater.* 56 (2007) 313-316.
- 39 C. Motz, T. Schöberl, R. Pippan, Mechanical properties of micro-sized copper bending beams machined by the focused ion beam technique, *Acta Materialia.* 53 (2005) 4269-4279.
- 40 D. Kiener, P. Hosemann, S.A. Maloy, A.M. Minor, In situ nanocompression testing of irradiated copper, *Nat Mater.* 10 (2011) 608-613.
- 41 Tabor, David. *The hardness of metals*. Oxford university press, 2000.
- [42] Mansur, L. K. "Correlation of neutron and heavy-ion damage: II. The predicted temperature shift if swelling with changes in radiation dose rate." *Journal of Nuclear Materials* 78.1 (1978): 156-160.
- [43] Hosemann, Peter, et al. "Issues to consider using nano indentation on shallow ion beam irradiated materials." *Journal of Nuclear Materials* 425.1 (2012): 136-139.

[44] Hardie, Christopher D., Steve G. Roberts, and Andy J. Bushby. "Understanding the effects of ion irradiation using nanoindentation techniques." *Journal of Nuclear Materials* 462 (2015): 391-401.

[45] T.Y. Tsui, G.M. Pharr, Substrate effects on nanoindentation mechanical property measurement of soft films on hard substrates, J. Mater. Res. 14 (1998) 292-301.

Table 1 - Elemental analysis provided by the manufacture and separate examination (compositions in weight percent). Data taken from ref.[4].

|                | Manufacturer | Chemical Analysis |
|----------------|--------------|-------------------|
| Cr             | 6.0          |                   |
| C              | 0.007        |                   |
| O <sub>2</sub> | 0.021        | 0.001             |
| N <sub>2</sub> | 0.0014       | 0.05              |
| P              |              | 0.005             |
| Ni             |              | 0.1               |
| Mn             |              | 0.02              |

Table 2 – Isotope activity measurements for Fe%6Cr sample irradiated in the ATR1 reactor at

INL.. Data provided by Collin Knight (INL).

| Isotope | Curies   | MBq   |
|---------|----------|-------|
| HE 6    | 0.00E+00 | 0.0   |
| BE 8    | 0.00E+00 | 0.0   |
| B 12    | 0.00E+00 | 0.0   |
| C 14    | 3.34E-09 | 0.0   |
| SC 47   | 1.29E-18 | 0.0   |
| SC 48   | 2.00E-25 | 0.0   |
| SC 49   | 0.00E+00 | 0.0   |
| TI 51   | 0.00E+00 | 0.0   |
| V 52    | 0.00E+00 | 0.0   |
| V 53    | 0.00E+00 | 0.0   |
| V 54    | 0.00E+00 | 0.0   |
| CR 51   | 9.91E-04 | 36.7  |
| CR 55   | 0.00E+00 | 0.0   |
| MN 54   | 7.50E-04 | 27.8  |
| MN 56   | 0.00E+00 | 0.0   |
| MN 57   | 0.00E+00 | 0.0   |
| MN 58   | 0.00E+00 | 0.0   |
| FE 55   | 3.42E-03 | 127.0 |
| FE 59   | 1.88E-04 | 7.0   |
| CO 60   | 3.57E-05 | 1.3   |
| CO 60M  | 0.00E+00 | 0.0   |
| CO 61   | 0.00E+00 | 0.0   |
| Y 90    | 4.02E-15 | 0.0   |
| Y 90M   | 0.00E+00 | 0.0   |
| Y 91    | 2.50E-09 | 0.0   |
| TOTAL   | 5.38E-03 | 199.8 |



Table 3 - Ion beam conditions for implantation with multiple energies at the Ion Beam Center, Rossendorf.

|                    |        |             |                 |
|--------------------|--------|-------------|-----------------|
| Target Temperature | 288 °C | Ion species | Fe <sup>+</sup> |
|--------------------|--------|-------------|-----------------|

| Energy<br>(MeV) | Dose<br>(ions/cm <sup>2</sup> ) | Ion<br>Charge | Dose Rate<br>(ions/cm <sup>2</sup> /s) | Beam Current<br>(nA/cm <sup>2</sup> ) | Time (hrs) |
|-----------------|---------------------------------|---------------|--|---------------------------------------|------------|
| 0.5             | 1.16 x 10 <sup>14</sup>         | 1             | 1.60 x 10 <sup>10</sup>                | 2.56                                  | 2.02       |
| 1               | 2.18 x 10 <sup>14</sup>         | 1             | 1.84 x 10 <sup>10</sup>                | 2.95                                  | 3.29       |
| 2               | 2.18 x 10 <sup>14</sup>         | 1             | 2.00 x 10 <sup>10</sup>                | 3.21                                  | 3.03       |
| 3               | 2.18 x 10 <sup>14</sup>         | 1             | 2.16 x 10 <sup>10</sup>                | 3.46                                  | 2.80       |
| 4.5             | 2.18 x 10 <sup>14</sup>         | 2             | 2.38 x 10 <sup>10</sup>                | 7.62                                  | 2.55       |
| 6               | 2.91 x 10 <sup>14</sup>         | 2             | 2.31 x 10 <sup>10</sup>                | 7.41                                  | 3.49       |
| 9               | 8.00 x 10 <sup>14</sup>         | 3             | 2.34 x 10 <sup>10</sup>                | 11.24                                 | 9.50       |

|       |                         |
|-------|-------------------------|
| TOTAL | 2.08 x 10 <sup>15</sup> |
|-------|-------------------------|

|       |       |
|-------|-------|
| TOTAL | 26.69 |
|-------|-------|

Table 4 - Fitting parameters for *equation 6.1* and correlation coefficient *R*.

|                    | $A_0$ ( $\mu\text{mGPa}$ ) | $A_1$ (GPa) | $R$  |
|--------------------|----------------------------|-------------|------|
| Un-irradiated      | 2.43                       | 0.477       | 0.90 |
| Ion-irradiated     | 1.88                       | 1.16        | 0.94 |
| Neutron-irradiated | 3.79                       | 1.29        | 0.91 |

Table 5 Dislocation loops found in ion irradiated and neutron irradiated samples, and obstacle strength calculations.

|                                    | Ion irradiation [9]                                   |   | Neutron irradiation [9,10]                                |  |
|------------------------------------|---|---|---|--|
|                                    | TEM   | APT   | APT   |  |
| Loop type                          | Mostly $\frac{1}{2}\langle 111 \rangle \{111\}$ -type | N/A   | Mostly $\frac{1}{2}\langle 111 \rangle \{111\}$ -type     |  |
| Segregating elements               | N/A   | Si along the dislocation lines with lower C and P but no Cr | Cr enriched at the periphery, Si located inside the loops | Both Si and Cr outside the dislocation loops |
| Size (nm)                          | 6.4   | 9.2   | 9.2   | 18.1   |
| Number density ( $/ 10^{22}/m^3$ ) | 1.3   | 1.4   | 2.9   |  |
|                                    | Ion Irradiation (Current work)                        |   | Neutron Irradiation (Current work)                        |  |
| $\lambda$ (nm)                     | 100   | 80  | 41  | 32   |
| Mean $\lambda$ (nm)                | 90  |   | 37  |  |
| $\Delta\tau_y$ (MPa)               | 170   |   | 500   |  |
| $\phi_c$ (eqn 1)                   | 42°   |   | 26°   |  |
| $\phi_c$ (eqn (2)                  | 50°   |   | 32°   |  |

**MeMicromechanical testingchanical properties and  
plasticity size effect and microstructural  
characterisation of Fe-6%Cr irradiated by Fe ions and  
by neutrons**

C.D. Hardie<sup>a, b</sup>, G.R. Odette<sup>c</sup>, Y. Wu<sup>c</sup>, S. Akhmadaliev<sup>d</sup> and S.G. Roberts<sup>a, b</sup>

<sup>a</sup> EURATOM/CCFE Association, Culham Centre for Fusion Energy (CCFE), Abingdon, Oxfordshire OX14 3DB, United Kingdom

<sup>b</sup> Department of Materials, University of Oxford, Oxford, OX1 3PH, United Kingdom

<sup>c</sup> UCSB Department of Mechanical Engineering, 2343 Engineering II Building, Santa Barbara, CA 93106-5070, United States of America

<sup>d</sup> Helmholtz-Zentrum Dresden-Rossendorf, Institute of Ion Beam Physics and Materials Research, D-01328 Dresden, Germany

Name: Christopher Hardie  
Address: Culham Centre for Fusion Energy (CCFE),  
Abingdon,  
Oxfordshire,  
OX14 3DB,  
United Kingdom  
Telephone Number: +44 (0)1235 46 4736  
Email Address: [chris.hardie@ukaea.uk](mailto:chris.hardie@ukaea.uk)

# 1 Introduction

The use of heavy ion implantation for the simulation of neutron irradiation under reactor conditions is common practice, due to the short time scales to reach relatively high damage levels and the absence of induced radioactivity; the latter avoids costly requirements for additional handling precautions and the use of hot cell facilities. However, there are issues with the correlation of the effects on microstructure and mechanical behaviour between ion implantation and neutron irradiation (usually from a fission reactor). Additionally, the use of either type of radiation for investigating likely response of materials within a fusion environment has limitations; for example, the deuterium-tritium fusion neutron energy spectrum includes a peak in neutron flux at 14.1 MeV, compared to lower energies in typical fission spectra, with few neutrons of energy higher than 5 MeV [1]. The fast fusion neutrons also produce significant levels of solid and gaseous transmutation products in structural materials such as steels, tungsten and SiC, which can be difficult to simulate, even with dual- and triple-beam ion irradiation facilities. [Therefore it is recognised that all sources of irradiation have specific characteristic effects on materials and the limitations of each type of irradiation must be accounted for when interpreting data.](#)

Mechanical testing of irradiated materials may be constrained by volume limitations: either by laboratory limits in handling radioactive material, or by the limited depth of the micron-scale damage layers typically produced by heavy ion ~~implantatio~~implantation. [The challenges in measuring mechanical properties of ion irradiated materials are discussed further in refs. \[43, 44\].](#) For the fusion materials community, small irradiation volumes are common amongst all concepts for Early Neutron Source ~~(ENS)~~ accelerator-driven high-energy neutron sources proposed in the EU 'roadmap to the realisation of fusion energy' [2]. It has long been established that the mechanical response of a material is not independent

of specimen size, particularly at small sizes [3]; therefore, the reduction of test specimen dimensions required to utilise these radiation sources presents a significant risk to the validity of data available.

This paper reports on a systematic study conducted on the effects of ion and neutron irradiation on the small-scale mechanical properties a model Fe-6%Cr alloy. The larger volume of radiation damage available in the neutron-irradiated material enabled the manufacture of micro-cantilever specimens with a wide range of sizes, providing an opportunity to investigate the effect of radiation damage on the mechanisms controlling the commonly observed size effect on measured strength. Samples were taken from a single batch of Fe 6%Cr alloy, irradiated with comparable doses and irradiation temperature, and tested by using identical nanoindentation and micro-cantilever methods.

## 2 Experimental Details

### 2.1 Material: Fe 6%Cr

A detailed description of the alloy manufacture and characterisation of the microstructure is given by Gelles [4]. A one hundred pound (~45 kg) heat of the Fe 6%Cr alloy was melted at the Paul D. Merica Research Laboratory in New York. Compositions provided by the manufacturer and chemical analysis performed by Lukens Steel Company (Pennsylvania) are given in *table 1*. The alloy was provided in the form of a 10mm diameter extruded bar, which was then rolled to approximately 3mm thickness.

The alloy was annealed under an argon atmosphere at 950 °C for 15 minutes followed by air cooling, then tempered at 750 °C, again followed by air cooling. This produced the microstructure shown in *figure 1*.

For the un-irradiated and ion irradiated material, sample polishing included a series of lapping stages using SiC abrasive papers from FEPA P120 to P4000 grades followed by a chemo-mechanical polish using a colloidal silica suspension (0.05  $\mu\text{m}$ ). The neutron-irradiated specimen was prepared by [Idaho National Laboratory \(INL\)](#) staff after irradiation. In order to reduce total activity, a 250- $\mu\text{m}$  thick, 2.3 mm diameter disc was punched from a larger sheet. The sample was ground with a series of abrasive papers to a final stage using FEPA P1200, polished using 3  $\mu\text{m}$  and 1  $\mu\text{m}$  diamond suspensions, followed by a chemo-mechanical polish using a colloidal silica suspension (0.05  $\mu\text{m}$ ).

## 2.2 Neutron Irradiation

A sample was irradiated in capsule 6A in the ATR1 materials test reactor in INL at a controlled temperature of 288  $^{\circ}\text{C} \pm 12^{\circ}\text{C}$ . The duration of the irradiation cycle was approximately 9 weeks and had a target total dose of 1.7 dpa. [The geometry of the sample used in this study is a 2 mm diameter disc ~200  \$\mu\text{m}\$  thick, corresponding to a volume of ~0.6  \$\text{mm}^3\$ .](#)

Formatted: Superscript

The total activity of the sample was measured at 199 MBq; *Table 2* shows the activity measurements for the sample. Dose rate measurements were 0.15 mSv/hr gamma (15 mrem/hr) and 0.9 mSv/hr beta (90 mrem/hr) on contact and 0.01 mSv/hr gamma (1 mrem/hr) at 30 cm.

## 2.3 Ion Irradiation

Ion implantations using iron ions were conducted at the [3 MV-Tandetron accelerator](#) ~~Ion Beam Centre~~ [at Helmholtz-Zentrum Dresden-Rossendorf](#) ~~in Rossendorf~~. The implantation was designed with multiple ion charges, energies and beam currents in an attempt to maintain a constant level of damage and dose rate with depth into the sample. [The beam](#)

[was scanned at ~1 kHz over the sample during irradiation.](#) The beam conditions used are shown in *table 3*.

The implantation temperature was measured and controlled at 288 °C by a thermocouple mechanically clamped adjacent to the samples on the base plate. The beam conditions were designed according to SRIM detailed calculation with full damage cascades [5] using a displacement energy for iron of 40 eV [6] and produced an average damage of 1.7 dpa in a layer 2 µm in depth from the sample surface as shown in *figure 2a*. Beam currents were set during implantation to give a consistent peak dose rate of  $5 \times 10^{-5}$  dpa/s for all energies (*figure 2b*).

## 2.4 Nanoindentation and Micro-Cantilever Testing

Nanoindentation was conducted with an MTS NANO Indenter XP (MTS NANO Oak Ridge Tennessee, USA) with a single Berkovich tip; the tip shape was calibrated before each test series. The “continuous stiffness measurement” (CSM) indentation and analysis method [7] was used to make at least 16 indents with a depth of 1000 nm in each sample, in arrays with a indent-to-indent spacing of 40 µm. [The amplitude and frequency of the CSM technique was 2 nm and 45 Hz respectively.](#) Due to the small grain size of the samples, data from each indent series, averaged across all indents, includes the response of several grains.

Micro-cantilevers were manufactured by Focused Ion Beam (FIB) milling in the un-irradiated and ion irradiated material using a Zeiss Auriga FIB/SEM dual beam system in the Department of Materials, Oxford University. Micro-cantilevers were manufactured in the neutron irradiated material using the ‘hot’ FEI Quanta dual beam microscope at the Center for Advanced Energy Studies ~~(CAES)~~ in Idaho Falls (USA). The following test specimens were produced:



- i. Neutron irradiated sample - 66 cantilevers with ~~depths~~ cross-sectional heights from 0.82 to 7.30  $\mu\text{m}$  (*figure 3*).
- ii. Ion irradiated sample - 30 cantilevers with cross-sectional heights ~~depths~~ from 0.36 to 2.3  $\mu\text{m}$
- iii. Un-irradiated sample - 32 cantilevers with cross-sectional heights ~~depths~~ from 0.53 to 5.11  $\mu\text{m}$

The cantilever beams were FIB milled by using various beam currents depending on the beam size and were finished with lower polishing currents to achieve a geometry with sharp edges. The

All beams were measured by stereo-imaging techniques using the principles described in *ref.* [8]. Tests were conducted using the Nano-XP nanoindenter by bending the beams to a final maximum peak strain (at the lower surface at the beam root),  $\varepsilon_{max}$ , of  $\sim 0.05$  and a target strain rate at the beam root surface of  $2 \times 10^{-4} \text{ s}^{-1}$ ; for the varying beam sizes, this required controlled displacement rates from 1.4 to 30  $\text{nm s}^{-1}$ . The stress-strain response from each test was calculated from the load-displacement data,  $P-\delta$ , measured with the nanoindenter. Maximum stress ~~and strain~~ for the triangular beams were calculated

by integrating the second moment of area for a triangular beam,  $= \frac{wh^3}{36}$ , with the equation for stress using simple beam theory,  $\sigma = \frac{My}{I}$ , where  $y = \frac{2h}{3}$ :

$$\sigma_{max} = \frac{24Pl}{wh^2} \quad (\text{eq. 1})$$

Similarly maximum strain was calculated by using eq.1 and  $\varepsilon = \frac{\sigma}{E}$  from Hooke's Law, and the equation for maximum deflection of a cantilever beam loaded at the free end  $\delta = \frac{Pl^3}{3EI}$  from simple beam theory:

$$\varepsilon_{max} = \frac{2\delta h}{l^2} \quad (\text{eq. 2})$$

where  $l$  is the distance between the beam's fixed end and the point of loading, and  $w$  is the beam width. The elastic modulus was calculated from the initial linear gradient of the stress-strain curve, and the proof stress was calculated as the stress at the point of interception between the stress-strain curve and a line with a gradient equal to the elastic modulus and x-intercept at 0.2% strain.

Errors were calculated by summing measuring and calculating all errors for elastic modulus and stress equations in quadrature:

$$\partial E = \sqrt{\left(\frac{E}{P}\right)^2 \partial P^2 + \left(\frac{3E}{l}\right)^2 \partial l^2 + \left(\frac{-E}{\delta}\right)^2 \partial \delta^2 + \left(\frac{-E}{w}\right)^2 \partial w^2 + \left(\frac{-3E}{h}\right)^2 \partial h^2} \quad (\text{eq. 3})$$

$$\partial \sigma = \sqrt{\left(\frac{\sigma}{P}\right)^2 \partial P^2 + \left(\frac{\sigma}{l}\right)^2 \partial l^2 + \left(\frac{-\sigma}{w}\right)^2 \partial w^2 + \left(\frac{-2\sigma}{h}\right)^2 \partial h^2} \quad (\text{eq. 4})$$

Each micro-cantilever test was modelled using [Finite Element Analysis \(FEA\)](#) to fit the simulation load-displacement curves to the experimental data by changing the modelled material's isotropic stress-strain properties, via a process of progressive convergent approximation. The continuum isotropic plasticity model used in FEA could not represent the stochastic nature of plasticity at the micron scale, hence the aim was to fit the model to the averaged experimental curve. A series of MATLAB functions was written to automate several tens of FEA simulations required for the fitting of data within a specified accuracy, and the final model isotropic stress-strain properties were recorded.

The radiation damage microstructures of these irradiated alloys have been characterised by Transmission Electron Microscopy (ion irradiated specimen) and Atom Probe Tomography (neutron and ion irradiated specimens). Results have been reported in detail elsewhere [9, 10], but are summarised in this paper when discussing likely hardening mechanisms.

## 3 Results

### 3.1 Nanoindentation

Nanoindentation data for elastic modulus versus indentation depth are shown in *figure 4a*. At shallow indentation depths the measured elastic moduli for ion and neutron irradiated materials are similar and are higher than for the un-irradiated material. As the indentation depth increases, the measured elastic modulus for the ion-irradiated material tends towards the values for the un-irradiated material, which correlates with an increasing influence on the measured modulus from the un-irradiated bulk substrate material below the ion-irradiated layer.

The modulus measured by the nanoindenter may be affected by errors in the tip to surface contact area calculated from the indenter displacement,  $h_c$ , and tip area function,  $f(h_c)$ , resulting from plastic pile-up of material surrounding the indents. Post-indentation contact area measurements of all indent impressions in the un-irradiated and neutron irradiated material were conducted by [Scanning Electron Microscopy \(SEM\)](#) imaging (*figure 5*). [This was done by measurement of the projected contact area, which is clearly visible by a sharp change in surface gradient \(edge\) of the indent pit using a similar method to that of Tsui et al. \[45\]. This area measurement is then used to calculate area-corrected values of hardness and elastic modulus using the same equations as reported in ref. \[7\].](#) Elastic modulus was then recalculated for the maximum indentation depth of 1000 nm using the measured post-indentation contact area for each indent; the average values with standard deviation are shown in *figure 4a* ("Area Correction" points). The use of actual contact area gives derived modulus values lower than those calculated from tip area functions; however modulus of

the neutron-irradiated material is still calculated to be ~15% greater than that of the unirradiated material.

*Figure 4b* shows average values for hardness versus indentation depth, and hardness values at maximum indentation depth corrected for post-indentation contact area measurement. Irradiation hardening is clearly evident in both irradiated alloys; however the hardening in the neutron-irradiated material is more than double that in the ion-irradiated material. Similar to the elastic modulus measurements, hardness in the ion-irradiated material tends towards the un-irradiated hardness as the indentation depth increases. Larger pile-up surrounding the indenter tip in the neutron-irradiated material results in a slight over estimation of irradiation hardening in calculations based on the tip area function; however pile-up in the ion-irradiated material may also overestimate the irradiation hardening.

Typical SEM images of indent impressions in the un-irradiated and neutron irradiated material are shown in *figure 5*. Plastically deformed material forming the pile-up lobes showed diffuse slip lines in the un-irradiated material and highly localised slip steps in the neutron-irradiated material. In both cases, slip lines were wavy and curved, rather than linear, indicating extensive cross slip of dislocations between available slip planes.

### **3.2 Micro-cantilever Testing**

Typical stress-strain curves for micro-cantilever tests of various sizes are shown in *figure 6*. For the un-irradiated material, as plastic deformation progresses, large load drops are visible, which tend to increase in magnitude as the beam sizes increase. Such load drops were not observed in either the ion- or neutron- irradiated alloys, where plastic deformation produced smooth variations in load. Very little work hardening was observed in the un-irradiated and ion-irradiated material and the stress-strain curves exhibit an almost perfectly

~~plastic response~~. In comparison, the neutron-irradiated material clearly exhibits work hardening.

The elastic modulus measurements with error bars calculated using the simple beam theory methods described in *section 2* are plotted in *figure 7* for all cantilever tests. A large scatter in the modulus between ~150 and 350\_GPa was observed in the smallest cantilevers, which may be partially attributed to variations in crystal orientation across each test (the elastic modulus of pure Fe varies from ~125\_GPa along the <100> axis to 275\_GPa along the <111> axis [11]). As the beam size increases, more grains contribute to the elastic modulus measurements and the scatter decreases; these values should tend towards approximately 210\_GPa, the macroscopic polycrystalline value [12]. The values of elastic modulus measured in the largest beams appear to be slightly lower than this value; this may be due to lower stiffness measurements caused by the deformation of material at the base of the beam and surrounding the indenter tip; this is not taken into account in the simple beam model, which assumes an purely elastic cantilever, rigidly fixed at one end.

The proof stresses calculated at 0.2% strain offset versus the beam height are plotted in *figure 8*. All three materials exhibit an increase in the measured proof stress as the cantilever size decreases. In the neutron-irradiated material, proof stress values above those for the unirradiated material are clearly evident across the entire range of beam sizes. In the ion-irradiated material the proof stress values for beams with  $h < 1 \mu\text{m}$  are not separable from those for unirradiated beams. For each material, it was found that the proof stress,  $\sigma_{proof}$ , could be fitted closely to a function of the form:

$$\sigma_{proof} = A_0 h^{-1} + A_1 \quad (\text{eq. 5})$$

where  $h$  is the beam height and  $A_1$  is the asymptotic value of proof stress ( $\sigma_{proof}$  at  $h = \infty$ ). The fitted curves are shown in *figure 8*. The values for  $A_0$  and  $A_1$  are given in *table 4* with the correlation coefficient  $R$ ; these values are discussed further in *section 4.3*.

Typical SEM images of the plastically deformed surfaces at the beam base are shown in *figure 9*. Slip steps are visible in the larger cantilever beams, but no slip steps were observable in the smallest beams. Large beams in the un-irradiated material exhibited only a few large slip steps in the deformed region. Slip steps in both types of irradiated material are more numerous and are well-separated, suggesting plasticity progresses inhomogeneously within localised slip planes.

### 3.3 Radiation damage microstructures

The radiation damage defect types, sizes and densities found in previous studies of these irradiated materials [9,10] are summarised in *Table 5*. The main points are that:

- 1) Dislocation loops are of  $\frac{1}{2}\langle 111 \rangle \{111\}$  type for both irradiation methods.
- 2) For the ion irradiated material, there is good agreement between the TEM and the APT measurements for the number density of loops:  $1.3$  to  $1.4 \times 10^{22} \text{ m}^{-3}$ .
- 3) The loop number density in the neutron irradiated material ( $2.9 \times 10^{22} \text{ m}^{-3}$ ) is roughly double that in the ion-irradiated material.
- 4) APT finds somewhat larger loops than TEM. Considering both techniques, typical loop diameters are  $\sim 6\text{-}9 \text{ nm}$  in ion-irradiated material, and bimodal in the neutron irradiated materials ( $\sim 9 \text{ nm}$  and  $\sim 18 \text{ nm}$ ).
- 5) Chromium segregation to the loops is found only in the neutron irradiated sample, but Si segregates (more weakly than chromium) to the loops for both irradiation types.

## 4 Discussion

The experiments reported in this paper were conducted with two objectives. The first objective was to assess the validation of ion implantation as an analogue for neutron irradiation, by means of a direct comparison. The second objective was to investigate the influence of irradiation hardening on the intrinsic size effects on sample strength, by conducting micro-mechanical testing with test specimens of various sizes. The implications of the results on both objectives are discussed below.

### 4.1 Hardening effects of radiation damage

The irradiation hardening due to damage from neutrons or ions can be considered in terms of interactions between mobile dislocations and the observed dislocation loops (and their associated solute clusters). If it is assumed that the loops act as local obstacles to dislocation motion, their effect on increasing the shear flow stress on the material (by  $\Delta\tau_y$ ) can be modelled as either:-

$$\Delta\tau_y = \frac{Gb}{\lambda} [\cos(\phi_c)]^{\frac{2}{3}} \quad \text{(eq. 8)}$$

Or

$$\Delta\tau_y = \frac{Gb}{\lambda} \cos(\phi_c) \quad \text{(eq. 9)}$$

where  $G$  is the material's shear modulus (82 GPa for iron),  $b$  is the length of the Burgers vector (0.248 nm),  $\lambda$  is the inter-obstacle spacing and  $2\phi_c$  is the critical angle subtended by the two arms of the dislocation as it breaks away from an obstacle. The parameter  $\phi_c$  characterises the obstacle strength, with low values implying a strong obstacle; at one limit, when  $\phi_c = 0$ , the obstacle is impenetrable, and the dislocation will pass the obstacle by the

Orowan bowing process, at the other limit, when  $\phi_c = 90^\circ$ , the dislocation passes the obstacle without hindrance. Equation (8), the “Friedel relation”, applies when obstacles are weak ( $\phi_c > \sim 50^\circ$ ), with the radius of dislocation line curvature under the applied stress being much greater than the typical inter-obstacle spacing [33, 34]; equation (9) applies when obstacles are strong ( $\phi_c \leq \sim 50^\circ$ ), with the radius of dislocation line curvature being of the same order as the typical inter-obstacle spacing [33].

The inter-obstacle spacing,  $\lambda$ , is determined as:

$$\lambda = [\rho \cdot d]^{-\frac{1}{2}} - d \quad (\text{eq. 10})$$

where  $\rho$  is the number of obstacles, of diameter  $d$ , per unit volume.

To obtain first-approximation values for  $\phi_c$  for the obstacles in the ion-irradiated and neutron irradiated materials, we use the nanoindentation data rather than the microcantilever data, as being less subject to scaling effects. Figure 4b indicates that the hardness increase due to ion-irradiation is  $\sim 1$  GPa and that due to neutron irradiation is  $\sim 3$  GPa; we take hardness as being  $\sim 3\times$  (tensile) yield stress [41], and shear flow stress as being  $\frac{1}{2}$  the yield stress (according to a maximum possible Schmid factor of 0.5 for a single crystal). Table 5, in the bottom 5 rows, shows results of these calculations (note that the data for defect sizes used for the ion-irradiated material were the mean value of those derived from TEM and APT data; for the neutron irradiated data, the mean of the values derived for the two loop sizes).

These rather crude calculations indicate that

- 1) the obstacle spacing is significantly less in the neutron-irradiated material than in the ion-irradiated material (even given the uncertainties in dealing with the bimodal size distribution in the neutron-irradiated material),



- 2) in both cases the loops are relatively strong obstacles, and are therefore best dealt with by equation (9).
- 3) the obstacle strength in the neutron irradiated material is significantly higher than in the ion-irradiated material.

The greater hardness increase due to neutron irradiation, compared with ion irradiation, thus results from both an increased dislocation loop density, and from the loops having greater obstacle strength to gliding dislocations. This greater obstacle strength in the neutron irradiated material is likely to be related to the higher level of segregation of chromium (and possibly silicon) to the dislocation loops. Greater obstacle strength in the neutron irradiated alloy is also consistent with the observation of work hardening in micro-cantilever tests, where it is possible that additional hardening features such as Orowan loops are produced when glissile dislocations overcome strong obstacles.

#### **4.2 Size Effects in Irradiated Materials**

The observed increase in mechanical strength of a material with decrease in test specimen size is a well-known phenomenon. The first observations of size dependence in tensile strength were made by Brenner in 1956 by tensile testing whiskers of iron, copper and silver from 1.2  $\mu\text{m}$  to 15  $\mu\text{m}$  in diameter [3]. There have been several attempts to characterise the underlying mechanisms which produce this effect, yet at present there is no clear explanation which can account for all of the various observations throughout the literature.

The mechanisms identified which result in size effects are:

- i. Strain gradient plasticity theory (beam bending and indentation)
- ii. Dislocation starvation
- iii. Dislocation truncation

iv. Dislocation pile-up at the beam neutral axis (beam bending only)

A variation of hardness with indentation depth is commonly observed in many materials and provides a method to measure the size dependence of strength in a single test. Nix and Gao [35] developed a law for strain gradient plasticity which suggests that the density of geometrically necessary dislocations (GNDs) required to support the shape of the indent impression is responsible for the indentation size effect (ISE). Assuming a simplified model comprising of a rigid conical indenter and deformation accommodated by circular GNDs in a hemispherical volume beneath the indenter tip, the density of GNDs is defined as [35]:

$$\rho_{GND} = \frac{3}{2bh} \tan^2 \theta \quad \text{(eq. 11)}$$

where  $\theta$  is the centreline-to-face angle of the indenter tip,  $b$  is the Burgers vector and  $h$  is the indentation depth. Thus, as the indenter is driven into the sample surface,  $\rho_{GND}$  and thereby the contribution to hardness due to work-hardening effects, decreases with indentation depth.

This theory does not apply to the strong size effect observed in micro-pillar tests [36], where there are no strain gradients produced from uniaxial loading. It has been proposed that the lack of dislocation multiplication events during the deformation of such small volumes may lead to a lack of available dislocations, termed dislocation starvation, and requires the nucleation of dislocations at a higher stress [37]. Similarly, dislocation sources require a characteristic volume to operate. The fabrication of test specimens may create surfaces which reduce the length of available dislocation segments and limit the volume available for source operation; these shorter segments and sources may require higher stresses to operate, known as truncation hardening [38].

The theories of source starvation and truncation suggest that plastic deformation is increasingly controlled by the activation characteristics of dislocation sources as the size of the test volume decreases. In the present work, there are two observations which indicate that the activation of dislocation sources influence plasticity in the tests. Firstly, discrete pop-in events in the load-displacement behaviour were observed during nanoindentation at small depths in several tests on all samples. This represents the transformation from elastic to fully plastic deformation by the activation of dislocation sources. Secondly, as commonly observed in other micro-mechanical tests [39], plasticity in the micro-cantilever tests shown in figure 6 progressed in a stochastic nature exhibiting several drops in load during mechanical testing. These load drops are likely to be related to the activation of individual sources as the deformation progresses.

As shown in figure 6a, the magnitude of the load drops increases with increasing beam size in the un-irradiated material. The magnitude of the load drop may be proportional to the strain accommodated once a dislocation source has been activated; it is likely that this strain is controlled by the number of dislocations which can be emitted before stresses produced by pile-up at the neutral axis cause the source to shut down. Hence, the increase in magnitude of the load drops with increasing beam size may relate to the longer distance dislocations glide on larger slip planes, which accommodate a greater number of dislocations emitted from a single source. This observation is supported by the appearance of visible slip steps at the surface only in the larger plastically deformed beams in figure 9, where each slip plane can accommodate a greater number of dislocations.

Load drops in cantilever tests indicate that the stress to activate dislocation sources dominates the observed strength of the material, resulting in no difference in the yield stress between the un-irradiated and ion-irradiated material for beams  $<1\text{ }\mu\text{m}$  depth. A similar

observation was made in the investigation conducted by Kiener et al. [40], where no irradiation hardening in proton irradiated Cu was measured in micro-pillar tests below a diameter of 400nm. However, even though the measured yield stress does not change with irradiation, strain localisation characteristics may differ; Kiener et al. identified that glissile dislocations partially or fully remove the irradiation-induced defects and that plastic deformation developed by localised slip within defect-free channels. The highly localised slip steps observed in the irradiated material around indents (*figure 5*) and at the deformed surfaces of micro-cantilevers (*figure 9*) suggests that the material investigated here deforms in a similar manner. This type of plastic deformation has been characterised for an ion-irradiated Fe 12%Cr alloy [20] and is caused by the annihilation of irradiation-induced defects by glissile dislocations. In the presence of high stresses produced to overcome size effect mechanisms, the defects may be annihilated without additional stress and plastic deformation progresses at the same stress as the un-irradiated material.

When the size of the test specimen increases above a critical size ( $\sim 1\text{ }\mu\text{m}$  in the present case), the stress determined by the size effect mechanisms is lower than that determined by the irradiation-induced defects and the response of the ion-irradiated material deviates from that of the un-irradiated material. In Kiener's study [40], this critical size was found to be a pillar diameter of 400nm, above which the yield stress of the irradiated Cu was apparently independent of size. This is clearly not observed in the tests reported here where the yield stress of the irradiated material continues to decrease as the beam depth increases.

Unlike the behaviour of ion-irradiated material, irradiation hardening measured for the neutron irradiated material was not completely obscured in the smallest beams. This suggests that the interaction between glissile dislocations and irradiation induced defects is different for the defects produced by ion-irradiation and those produced by neutron-

irradiation. As suggested in *section 4.1*, the neutron-irradiated material is likely to exhibit Cr enrichment associated with radiation damage dislocation loops. Unlike the “clean” dislocation loops, areas of Cr enrichment cannot annihilate by reaction with a glissile dislocation, and thus will contribute to the stress required for plastic deformation in addition to the mechanisms controlling the size effect. Furthermore, the increased work hardening behaviour observed in the neutron-irradiated material indicates the resistance to annihilation of Cr enriched regions.

### **4.3 Comparison with Macro-Scale Properties**

The Fe 6%Cr material studied here was also investigated by Vickers micro-hardness testing. A LECO LM247 AT instrument was operated with a load of 500 g, to produce indents into both the un-irradiated and neutron irradiated material. Values of hardness were 117.2 Hv (+/- 2.7) for the un-irradiated material and 232.9 Hv (+/- 5.8) for the neutron-irradiated material. According to the empirical relationships derived for irradiated austenitic and ferritic steels [41], dividing these values by 3.03 (see ref. [41]) provides an estimate of the macro scale yield stress; this produces a yield stress of 355.83 MPa for the un-irradiated material and 706.62 MPa for the neutron-irradiated material. Using the same technique on the nanoindentation measured hardness at the maximum displacement of 1000 nm produces hardness values of ~500 MPa for the un-irradiated material and ~1000 MPa for the neutron irradiated material, suggesting that the results are subject to indentation size effect.

The micro-cantilever data described in *section 3.2* may provide a means for extrapolation to macro scale properties. The observation that the proof stress is strongly proportional to  $h^{-1}$  was also made by Motz et al. [39] for micro-cantilever tests in a copper single crystal. Motz

provided an analytical model which accounts for the increase in flow stress produced by the pile-up of dislocations at the neutral axis. This contribution,  $\sigma_{PU}$ , is given by:

$$\sigma_{PU} = \frac{\alpha G}{b} \frac{\omega^2}{x^2} h \lambda^2 \quad (\text{eq. 12})$$

where  $\alpha$  is a constant (0 to 1),  $G$  is the shear modulus (84 GPa for iron),  $b$  is the Burgers vector (248 pm for iron),  $\omega$  is the beam bending angle,  $x$  is the size of the plastically deformed region,  $h$  is the beam height and  $\lambda$  is the dislocation source spacing. The assumption that the size of the plastically deformed region can be approximated as the beam thickness<sup>1</sup> ( $x = h$ ) gives [39]:

$$\sigma_{PU} = \frac{\alpha G}{b} \frac{\omega^2}{h} \lambda^2 \quad (\text{eq. 13})$$

According to the equations in section 3.2, values of  $A_0$  may be described by:

$$A_0 = \frac{\alpha G}{b} \omega^2 \lambda^2 \quad (\text{eq. 14})$$

Using the fitted values for  $A_0$  in table 4 produces an average dislocation source spacing from ~20 nm to ~200 nm for the three materials at values of  $\alpha$  from 0.1 to 0.9. This range corresponds well with the distribution of slip steps in the deformed beams shown in figure 9.

The values for  $A_1$  in table 4 represents the asymptotic values of proof stress ( $\sigma_{proof}$  at  $h = \infty$ ) of 477 MPa for the un-irradiated and 1290 MPa for the neutron irradiated material, which is similar to the yield stress calculated from nanoindentation hardness as described

---

<sup>1</sup> A large extent of the plastically deformed region is more likely to be confined within the bottom half of the beam, however the entire beam thickness is assumed here for consistency with the method developed by Motz et al. [39]

above. These values are larger than the values of yield stress calculated from the Vickers hardness data and indicate that additional size effect mechanisms such as source starvation/truncation may also contribute to the response of the material. This suggests that the extrapolation of yield stress to macro scale properties requires a more complex model of the mechanisms which contribute to the size effect or a larger range of test sizes.

#### **4.4 Comparison of Ion and Neutron Irradiation**

The production and evolution of radiation damage in a given material depends on several parameters including the type and energy of the irradiating particle, the fluence / dose (number of displacements, dpa), the irradiation temperature and flux/dose rate (damage rate, dpa/s) [13]. The current experiment produced neutron and ion irradiated materials with planned dose of 1.7dpa and irradiation temperature of 288 °C, yet the nanoindentation measurements presented in *figure 4b* and micro-cantilever results in *figure 8* show clear differences between hardening produced by irradiation with ions and that with neutrons. These differences might be caused by inconsistencies in damage calculations, the different PKA energy spectra between the two irradiation types, the presence of transmutation He and H in neutron-irradiated materials only, or by differences in damage types and densities produced by irradiation at different dose rates.

##### **4.4.1 Damage Calculations – Neutron Irradiation**

Three different methods were used to calculate the level of radiation damage in the neutron irradiated alloy:

**Method 1:** The dose was calculated using the damage rate equation [14] and post irradiation fluence measurements as a function of neutron energy,  $\phi(E_i)$ , and the energy-dependent displacement cross-section,  $\sigma_D(E_i)$ , for the neutron irradiated material produced at INL. :

$$R_d = N \int_E^E \phi(E_i) \sigma_D(E_i) dE_i \quad (\text{eq. 6})$$

This produced a dose value of **1.83dpa**.

**Method 2:** The PKA energy (recoil) spectra for the neutron irradiated material were calculated using the NJOY-2012 code [15] (to produce recoil probability matrices,  $\sigma(E_i, T)$  defined in *equation 2.3*) and SPECTER (to collapse these matrices with the ATR1 spectrum). The PKA energy spectra for the dominant reactions during irradiation are plotted in *figure 10*. The results from a FISPACT-II inventory simulation [16] produced a value for total damage of **1.63dpa**.

**Method 3:** The damage energy,  $T$ , as a function of PKA energy,  $E_i$ , in iron was calculated using the data and relationships produced by Dierckx [17]; this is shown in *figure 11*. The damage energy was used with the modified Kinchin and Pease NRT formula [18]:

$$dpa_{NRT} = \frac{0.8T}{2Ed} \quad (\text{eq. 7})$$

This method produced a value for total damage of **1.72dpa**.

All three values are thus reasonably consistent at 1.7\_dpa, +/-0.1\_dpa.

#### 4.4.2 Damage Calculations – Ion Irradiation

For the configuration of the ion implantations, doses were calculated by using the ‘Detailed Calculation with Full Damage Cascades’ model in SRIM as shown in *figure 2*, producing a uniform damage layer with an average damage of 1.7\_dpa over 2μm. However, the



application of method 3, by using the same damage energy function produced by Dierckx [17] and NRT formula produces a value of ~0.5\_dpa. This discrepancy is caused by inconsistencies in the SRIM codes, as has been confirmed by Stoller et al. [19]. As recommended by Stoller, the 'Quick Calculation of Damage' (Kinchin-Pease) model in SRIM was used to calculate the actual ion implantation dose. The damage energy,  $T$ , was calculated by:

$$T = E_i^0 - E_i^I - E_T^I = E_i^P + E_i^B + E_T^P + E_T^B, \quad (\text{eq. 8})$$

where the energy of the incident ion is distributed into electronic stopping (superscript  $I$ ), lattice binding energy (superscript  $B$ ) and lattice phonons (superscript  $P$ ), from the incident ions (subscript  $i$ ) or the target atoms (subscript  $t$ ). In order to remain consistent with the NRT model used for the neutron irradiation, the lattice binding energy was set to zero and the number of phonons/Å-ion was used to give  $T$ . This produced an average damage with depth of 0.82\_dpa and is shown with the original target of 1.7\_dpa in *figure 12*.

Thus it is likely that the neutron irradiated alloy was physically subjected to more displacement damage, which may have contributed to the higher number of defects and segregation of Cr observed for this material. However, several ion implantation studies of similar alloys have identified that irradiation hardening saturates at a doses of 1-2\_dpa (calculated by using the 'Detailed Calculation with full Damage Cascades' model) [20,21]. Thus, a variation in dose alone is unlikely to explain the large difference in hardening between the ion and neutron irradiated materials.

#### **4.4.3 The Effect of PKA Energy Spectra**

Fission neutrons produce PKA energies of up to 200 keV [17] and have an energy spectrum which includes a tail of lower energies. In comparison, in ion implantation experiments each

incident ion simulates a PKA with an energy equal to that of the beam energy (up to 9 MeV in the current experiment) [22,23]. Using recoil spectra for  $^{56}\text{Fe}$  and calculations of displacements from method 3 above, the damage as a function of PKA energy produced by the ion and neutron irradiations is shown in *figure 13*.

The difference in the total number of displacements produced by each incident particle should be accounted for in the damage calculations for each irradiation; thus, areas beneath the curves for ions and neutrons in *figure 13* should be equal to the total dose calculated for each method. However, the types of primary defects produced by an incident ion or neutron may differ depending on the PKA energy. There is agreement amongst several authors [17, 24-26] that above a threshold damage energy of approximately 5 to 10 KeV, the production of primary defects in a material is independent of damage energy. The threshold energy represents the transition from the production of Frenkel pairs at the lowest PKA energies to larger cascades and sub-cascade formation at higher PKA energies. Above this threshold energy, formations of separate sub-cascades produce the same primary defect types and the numbers of these defects remain a constant function of the energy (30% of the NRT value [26]). On the other hand, recent MD simulations [27] identified that cascades were in the form of a continuous distribution of damage and that the primary defect morphology continues to change as a function of energy up to 0.5 MeV.

For the neutron irradiation, the majority of the damage was produced by PKA energies from ~60 to 275 keV with a peak at 158 keV. In contrast, PKA energies produced during the ion implantation were 0.5 to 9 MeV. This suggests that the cascade damage morphology produced by the fission neutrons may be significantly different to that produced by ion implantation. This is likely to influence the fraction of freely migrating defects in both ion and neutron irradiations [28, 29]; that is, the fraction of isolated point defects or defects

within small clusters which are mobile. The fraction of freely migrating defects produced within an irradiated material will directly influence diffusion mediated processes such as creep, swelling and radiation induced segregation (RIS). In the current experiment, differences in the PKA energies between the ion and neutron irradiated sample may have contributed to the observed RIS of Cr in the neutron irradiated sample. The influence of freely migrating defects is also determined whether on average they recombine and annihilate, or agglomerate to form dislocation loops or voids, or migrate to sinks such as grain boundaries etc. This is directly influenced by dose rate as described below.

#### **4.4.4 The Effect of Dose Rate**

The dose rate of the ion-implantation was approximately 500 times higher than for the neutron irradiation. The rate of interaction between cascade defects is dependent on defect mobility and is proportional to the square of the defect density. The lower dose rate neutron irradiation results in a lower defect density in a given volume per unit time; this may result in a lower number of defect interactions and an increase in the length of defect migration paths compared to higher dose rates. Increasing rates of irradiation creep and swelling with decreasing dose rate have been shown for austenitic steels [30, 31]. More recently an increase in irradiation hardening at lower dose rates was shown in ion-irradiated Fe-Cr alloys of similar composition [32]; [here it was shown](#) that heightened Cr segregation was the cause of additional hardening in the alloy irradiated with the lowest dose rate. The observation of Cr segregation described in section 3.3 and table 5, is comparable to that reported in ref. [32] and thus is likely to have been the primary cause of higher irradiation hardening produced by neutron irradiation compared to ion irradiation.

[As discussed, the variation in the effects of irradiation with different dose rates has been identified elsewhere. Methods to overcome variation in dose rate have been proposed, such](#)

as the use of a temperature shift to manipulate defect mobility and accommodate a different dose rate [42]. However, radiation produces several types of defect all with a characteristic mobility which cannot be accommodated by a single temperature shift. A temperature shift may therefore not facilitate the complete comparison of irradiations conducted at different rates accurately. This is discussed further in section 4.2.

#### 4.4.5 Transmutation He and H

In addition, the FISPACT-II inventory simulation indicated that approximately 10 appm He and 6.5 appm H was produced in the alloy during neutron irradiation. This may have also contributed to the increase in irradiation hardening.

### 4.5 Hardening effects of radiation damage

The irradiation hardening due to damage from neutrons or ions can be considered in terms of interactions between mobile dislocations and the observed dislocation loops (and their associated solute clusters). If it is assumed that the loops act as local obstacles to dislocation motion, their effect on increasing the shear flow stress on the material (by  $\Delta\tau_y$ ) can be modelled as either:

$$\Delta\tau_y = \frac{Gb}{\lambda} [\cos(\phi_c)]^{\frac{2}{3}} \quad (eq. 8)$$

Or

$$\Delta\tau_y = \frac{Gb}{\lambda} \cos(\phi_c), \quad (eq. 9)$$

where  $G$  is the material's shear modulus (82 GPa for iron),  $b$  is the length of the Burgers vector (0.248 nm),  $\lambda$  is the inter obstacle spacing and  $2\phi_c$  is the critical angle subtended by the two arms of the dislocation as it breaks away from an obstacle. The parameter  $\phi_c$  characterises the obstacle strength, with low values implying a strong obstacle; at one limit,

when  $\phi_e = 0$ , the obstacle is impenetrable, and the dislocation will pass the obstacle by the Orowan bowing process, at the other limit, when  $\phi_e = 90^\circ$ , the dislocation passes the obstacle without hindrance. Equation (9), the "Friedel relation", applies when obstacles are weak ( $\phi_e > 50^\circ$ ), with the radius of dislocation line curvature under the applied stress being much greater than the typical inter obstacle spacing [23, 24]; equation (9) applies when obstacles are strong ( $\phi_e < 50^\circ$ ), with the radius of dislocation line curvature being of the same order as the typical inter obstacle spacing [23].

The inter obstacle spacing,  $\lambda$ , is determined as:

$$\lambda = [\rho \cdot d]^{-\frac{1}{2}} \cdot d \quad \text{(eq. 10)}$$

where  $\rho$  is the number of obstacles, of diameter  $d$ , per unit volume.

To obtain first approximation values for  $\phi_e$  for the obstacles in the ion irradiated and neutron irradiated materials, we use the nanoindentation data rather than the microcantilever data, as being less subject to scaling effects. Figure 4b indicates that the hardness increase due to ion irradiation is  $\sim 1$  GPa and that due to neutron irradiation is  $\sim 3$  GPa; we take hardness as being  $\sim 3\times$  (tensile) yield stress, and shear flow stress as being  $\frac{1}{2}$  the yield stress. Table 5, in the bottom 5 rows, shows results of these calculations (note that the data for defect sizes used for the ion irradiated material were the mean value of those derived from TEM and APT data; for the neutron irradiated data, the mean of the values derived for the two loop sizes). These rather crude calculations indicate that

- 4) the obstacle spacing is significantly less in the neutron irradiated material than in the ion irradiated material (even given the uncertainties in dealing with the bimodal size distribution in the neutron irradiated material),

- 5) in both cases the loops are relatively strong obstacles, and are therefore best dealt with by equation (9);
- 6) the obstacle strength in the neutron irradiated material is significantly higher than in the ion irradiated material.

The greater hardness increase due to neutron irradiation, compared with ion irradiation, thus results from both an increased dislocation loop density, and from the loops having greater obstacle strength to gliding dislocations. This greater obstacle strength in the neutron irradiated material is likely to be related to the higher level of segregation of chromium (and possibly silicon) to the dislocation loops. Greater obstacle strength in the neutron irradiated alloy is also consistent with the observation of work hardening in micro cantilever tests, where it is possible that additional hardening features such as Grown loops are produced when glissile dislocations overcome strong obstacles.

#### 4.6 Size Effects in Irradiated Materials

The observed increase in mechanical strength of a material with decrease in test specimen size is a well known phenomenon. The first observations of size dependence in tensile strength were made by Brenner in 1956 by tensile testing whiskers of iron, copper and silver from 1.2 $\mu\text{m}$  to 15 $\mu\text{m}$  in diameter [3]. There have been several attempts to characterise the underlying mechanisms which produce this effect, yet at present there is no clear explanation which can account for all of the various observations throughout the literature. The mechanisms identified which result in size effects are:

- v. Strain gradient plasticity theory (beam bending and indentation)
- vi. Dislocation starvation
- vii. Dislocation truncation

~~viii. Dislocation pile up at the beam neutral axis (beam bending only)~~

~~A variation of hardness with indentation depth is commonly observed in many materials and provides a method to measure the size dependence of strength in a single test. Nix and Gao [35] developed a law for strain gradient plasticity which suggests that the density of geometrically necessary dislocations (GNDs) required to support the shape of the indent impression is responsible for the indentation size effect (ISE). Assuming a simplified model comprising of a rigid conical indenter and deformation accommodated by circular GNDs in a hemispherical volume beneath the indenter tip, the density of GNDs is defined as:~~

$$\rho_{GND} = \frac{3}{2bh} \tan^2 \theta \quad \text{(eq. 11)}$$

~~where  $\theta$  is the centreline to face angle of the indenter tip,  $b$  is the Burgers vector and  $h$  is the indentation depth. Thus, as the indenter is driven into the sample surface,  $\rho_{GND}$ , and thereby the contribution to hardness due to work hardening effects, decreases with indentation depth.~~

~~This theory does not apply to the strong size effect observed in micro-pillar tests [36], where there are no strain gradients produced from uniaxial loading. It has been proposed that the lack of dislocation multiplication events during the deformation of such small volumes may lead to a lack of available dislocations, termed dislocation starvation, and requires the nucleation of dislocations at a higher stress [37]. Similarly, dislocation sources require a characteristic volume to operate. The fabrication of test specimens may create surfaces which reduce the length of available dislocation segments and limit the volume available for source operation; these shorter segments and sources may require higher stresses to operate, known as truncation hardening [38].~~

The theories of source starvation and truncation suggest that plastic deformation is increasingly controlled by the activation characteristics of dislocation sources as the size of the test volume decreases. In the present work, there are two observations which indicate that the activation of dislocation sources influence plasticity in the tests. Firstly, discrete pop-in events in the load-displacement behaviour during nanoindentation at small depths, represents the transformation from elastic to fully plastic deformation by the activation of dislocation sources. Secondly, as commonly observed in other micro-mechanical tests [39], plasticity in the micro-cantilever tests shown in figure 6 progressed in a stochastic nature exhibiting several drops in load during mechanical testing. These load drops are likely to be related to the activation of individual sources as the deformation progresses.

As shown in figure 6a, the magnitude of the load drops increases with increasing beam size in the un-irradiated material. The magnitude of the load drop may be proportional to the strain accommodated once a dislocation source has been activated; it is likely that this strain is controlled by the number of dislocations which can be emitted before stresses produced by pile-up at the neutral axis cause the source to shut down. Hence, the increase in magnitude of the load drops with increasing beam size may relate to the longer distance dislocations glide on larger slip planes, which accommodate a greater number of dislocations emitted from a single source. This observation is supported by the appearance of visible slip steps at the surface only in the larger plastically deformed beams in figure 9, where each slip plane can accommodate a greater number of dislocations.

Load drops in cantilever tests indicate that the stress to activate dislocation sources dominates the observed strength of the material, resulting in no difference in the yield stress between the un-irradiated and ion-irradiated material for beams  $< 1\mu\text{m}$  depth. A similar observation was made in the investigation conducted by Kiener et al. [40], where no



irradiation hardening in proton irradiated Cu was measured in micro-pillar tests below a diameter of 400nm. However, even though the measured yield stress does not change with irradiation, strain localisation characteristics may differ; Kiener et al. identified that glissile dislocations partially or fully remove the irradiation induced defects and that plastic deformation developed by localised slip within defect free channels. The highly localised slip steps observed in the irradiated material around indents (figure 5) and at the deformed surfaces of micro-cantilevers (figure 9) suggests that the material investigated here deforms in a similar manner. This type of plastic deformation has been characterised for an ion irradiated Fe 12%Cr alloy [20] and is caused by the annihilation of irradiation induced defects by glissile dislocations. In the presence of high stresses produced to overcome size effect mechanisms, the defects may be annihilated without additional stress and plastic deformation progresses at the same stress as the un irradiated material.

When the size of the test specimen increases above a critical size ( $\sim 1\mu\text{m}$  in the present case), the stress determined by the size effect mechanisms is lower than that determined by the irradiation induced defects and the response of the ion irradiated material deviates from that of the un irradiated material. In Kiener's study [40], this critical size was found to be a pillar diameter of 400nm, above which the yield stress of the irradiated Cu was apparently independent of size. This is clearly not observed in the tests reported here where the yield stress of the irradiated material continues to decrease as the beam depth increases.

Unlike the behaviour of ion irradiated material, irradiation hardening measured for the neutron irradiated material was not completely obscured in the smallest beams. This suggests that the interaction between glissile dislocations and irradiation induced defects is different for the defects produced by ion irradiation and those produced by neutron irradiation. As suggested in section 4.1, the neutron irradiated material is likely to exhibit Cr

enrichment associated with radiation damage dislocation loops. Unlike the “clean” dislocation loops, areas of Cr enrichment cannot annihilate by reaction with a glissile dislocation, and thus will contribute to the stress required for plastic deformation in addition to the mechanisms controlling the size effect. Furthermore, the increased work hardening behaviour observed in the neutron irradiated material indicates the resistance to annihilation of Cr enriched regions.

#### 4.7 Comparison with Macro-Scale Properties

The Fe-6%Cr material studied here was also investigated by Vickers micro hardness testing. A LECO LM247 AT instrument was operated with a load of 500g, to produce indents into both the un-irradiated and neutron irradiated material. Values of hardness were 117.2Hv (+/- 2.7) for the un irradiated material and 232.9Hv (+/- 5.8) for the neutron irradiated material. According to the empirical relationships derived for irradiated austenitic and ferritic steels [41], dividing these values by 3.03 provides an estimate of the macro scale yield stress; this produces a yield stress of 355MPa for the un irradiated material and 706MPa for the neutron irradiated material.

The micro cantilever data described in section 3.2 may provide a means for extrapolation to macro scale properties. The observation that the proof stress is strongly proportional to  $h^{-1/2}$  was also made by Motz et al. [29] for micro cantilever tests in a copper single crystal. Motz provided an analytical model which accounts for the increase in flow stress produced by the pile-up of dislocations at the neutral axis. This contribution,  $\sigma_{pu}$ , is given by:

$$\sigma_{pu} = \frac{\alpha G \omega^2}{b \lambda^2} h \lambda^2 \quad (\text{eq. 12})$$

where  $\alpha$  is a constant (0 to 1),  $G$  is the shear modulus (84GPa for iron),  $b$  is the Burgers vector (248pm for iron),  $\omega$  is the beam bending angle,  $x$  is the size of the plastically deformed region,  $h$  is the beam height and  $\lambda$  is the dislocation source spacing. The assumption that the size of the plastically deformed region can be approximated as the beam thickness<sup>2</sup> ( $x = h$ ) gives [39]:

$$\sigma_{PD} = \frac{\alpha G \omega^2}{b} \lambda^2 \quad (\text{eq. 13})$$

According to the equations in section 3.2, values of  $A_0$  may be described by:

$$A_0 = \frac{\alpha G}{b} \omega^2 \lambda^2 \quad (\text{eq. 14})$$

Using the fitted values for  $A_0$  in table 4 produces an average dislocation source spacing from  $\sim 20\text{nm}$  to  $\sim 200\text{nm}$  for the three materials at values of  $\alpha$  from 0.1 to 0.9. This range corresponds well with the distribution of slip steps in the deformed beams shown in figure 9.

The values for  $A_\infty$  in table 4 represents the asymptotic values of proof stress ( $\sigma_{proof}$  at  $h = \infty$ ) of 477MPa for the un-irradiated and 1290MPa for the neutron irradiated material. These values are larger than the values of yield stress calculated from the Vickers hardness data and indicate that additional size effect mechanisms such as source starvation/truncation may also contribute to the response of the material. This suggests that the extrapolation of yield stress to macro scale properties requires a more complex model of the mechanisms which contribute to the size effect or a larger range of test sizes.

---

<sup>2</sup> A large extent of the plastically deformed region is more likely to be confined within the bottom half of the beam, however the entire beam thickness is assumed here for consistency with the method developed by Motz et al. [39]

## 5 Summary

- i. Fe<sub>6</sub>Cr irradiated to a nominal dose of 1.7 dpa at 288 °C exhibited significantly different irradiation hardening depending on whether the irradiation was by ions or by neutrons.
  - a. Nanoindentation results showed that irradiation hardening in the neutron-irradiated material was ~3 GPa, whilst it was ~1 GPa in the ion-irradiated material.
  - b. Unlike the un-irradiated and ion-irradiated material, the neutron-irradiated material exhibited some work hardening in micro-cantilever tests.
- ii. The variation of hardening may be caused by:
  - a. Inconsistencies in damage calculations between the standard NRT formula for neutron irradiations and 'detailed calculation with full damage cascades' model in TRIM for ion-irradiation. As described in *section 4.14.2*, comparison with similar work suggests that the ion implantation damage is likely to be at or near saturation.
  - b. A difference in the characteristics of the radiation damage introduced by the two radiation types has been observed; principally a higher density of dislocation loops in the neutron irradiated material ( $2.9 \times 10^{22} \text{ m}^{-3}$ ) compared to the ion irradiated material ( $1.4 \times 10^{22} \text{ m}^{-3}$ ) and a tendency for Cr clustering in the neutron irradiated material. This clustering is likely to be associated with the dislocation loops, making them stronger obstacle to dislocation motion, and more resistant to removal by the passage of mobile dislocations.

- c. The presence of the enhanced Cr enriched regions in the neutron irradiated material may results from differences in the dose rate ( $5 \times 10^{-5}$  dpa/s for ion-irradiation and  $\sim 3 \times 10^{-7}$  dpa/s for neutron-irradiation) and/or PKA energy spectra (see *figure 13*).
- iii. All materials exhibited a size effect with yield stress varying by up to 700% for beam depths from  $\sim 0.5 \text{ }\mu\text{m}$  to  $\sim 7 \text{ }\mu\text{m}$  (*figure 8*). The effect in the ion-irradiated material was such that hardening due to irradiation was obscured by size effects. In the neutron irradiated material, the stronger hardening due to irradiation was not fully obscured by size effects. These differences in strength and irradiation hardening are likely to have been caused by the different types of defect produced by the ion and neutron irradiations, in particular a stronger tendency to produce chromium enriched regions for the neutron irradiation where the dose rate is much lower than for ion irradiation.
- iv. Attempts to extrapolate micro-cantilever results to the macro-scale in *section 4.3* appear unsuccessful. This is likely to be caused by errors in empirical relationships used for Vickers hardness data and/or multiple size effect mechanisms including source activation and dislocation pile-up at the neutral axis, which require a more complex model.

## 6 Acknowledgements

Work on the neutron irradiated sample was supported by the National Scientific User Facility (NSUF) and the Center for Advanced Energy Studies-Microscopy and Characterization Suite (CAES-MaCS); in particular we thank Jatuporn Burns for assistance with the FIB at CAES-MaCS. The authors thank Mr J.W. Nielsen at INL for supplying post irradiation fluence

measurements as a function of neutron energy,  $\phi(E_i)$ , and the energy-dependent displacement cross-section,  $\sigma_D(E_i)$ , for the neutron irradiated material. Thanks to Dr M. Gilbert at UKAEA for providing damage calculations using NJOY, SPECTER and FISPACT codes. Thanks to Mr T Milot at INL for supplying Vickers hardness data. The work reported here was partially supported by the Engineering and Physical Science Council (EPSRC) via a Programme Grant “Materials for Fusion and Fission Power”, EP/H018921. C.D. Hardie thanks EPSRC and the Culham Centre for Fusion Energy (CCFE) for funding in the form of an Industrial CASE studentship.

## References

- 1 R.E. Stoller, L.R. Greenwood, Subcascade formation in displacement cascade simulations: Implications for fusion reactor materials, *J. Nucl. Mater.* 271-272 (1999) 57-62.
- 2 F. Romanelli, P. Barabaschi, D. Borba, G. Federici, L. Horton, R. Neu, D. Stork, H. Zohm, Fusion Electricity: A roadmap to the realisation of fusion energy. EFDA Report (2013)
- 3 S.S. Brenner, Tensile strength of whiskers, *J. Appl. Phys.* 27 (1956) 1484-1491.
- 4 D.S. Gelles, Microstructural examination of neutron-irradiated simple ferritic alloys, *J. Nucl. Mater.* 108-109 (1982) 515-526.
- 5 J.F. Ziegler, M.D. Ziegler, J.P. Biersack, SRIM – The stopping and range of ions in matter (2010), *Nucl. Instrum. Methods.* B268 (2010) 1818-1823.
- 6 Standard Practice for Measurement of Mechanical Properties during Charged-Particle Irradiation. ASTM International E821 - 96(2009).
- 7 W.C. Oliver, G.M. Pharr, An improved technique for determining hardness and elastic modulus using load and displacement sensing indentation experiments., *J Mater Res.* 7 (1992) 1564-1583.
- 8 G. Piazzesi, Photogrammetry with the scanning electron microscope, *J. Phys. E: Sci. Instrum.* 6 (1973) 392-396.
- 9 Y. Wu, P. Wells, G. R. Odette, T. Yamamoto, S. Roberts, C. Hardie, D. Bhattacharyya, M. Bachhav and E. A. Marquis, Microstructural characterization of a Fe+ irradiated Fe-6%Cr alloy, US Department of Energy Report on the Fusion Reactor Materials Program, 2015, DOE/ER-0313/58, pp 8-11.
- 10 M. Bachhav, L. Yao, G. R. Odette, E. A. Marquis, *J. Nucl. Mater.* 453 (2014) 334.
- 11 G.E. Dieter, *Mechanical metallurgy*, McGraw-Hill New York, 1976.
- 12 G. Speich, A. Schwoeble, W. Leslie, Elastic constants of binary iron-base alloys, *Metallurgical Transactions.* 3 (1972) 2031-2037.
- 13 C. Abromeit, Aspects of simulation of neutron damage by ion irradiation, *J. Nucl. Mater.* 216 (1994) 78-96.
- 14 G.S. Was, *Fundamentals of radiation materials science: metals and alloys*, Springer, 2007.
- 15 R. MacFarlane, D. Muir, The NJOY nuclear data processing system, Los Alamos National Laboratory LA-UR-12-27079 (2012).
- 16 J. Sublet, J. Eastwood, J. Morgan, The FISPACT-II User Manual CCFE-R(11)11 Issue 3, Tech. Rep. CCFE (2012).
- 17 R. Dierckx, The importance of the PKA-energy spectrum for radiation damage simulation, *J. Nucl. Mater.* 144 (1987) 214-227.
- 18 M.J. Norgett, M.T. Robinson, I.M. Torrens, A proposed method of calculating displacement dose rates, *Nucl. Eng. Des.* 33 (1975) 50-54.
- 19 R.E. Stoller, M.B. Toloczko, G.S. Was, A.G. Certain, S. Dwaraknath, F.A. Garner, On the use of SRIM for computing radiation damage exposure, *Nuclear instruments and methods in physics research section B: beam interactions with materials and atoms* 310 (2013): 75-80.
- 20 C.D. Hardie, S.G. Roberts, Nanoindentation of model Fe–Cr alloys with self-ion irradiation, *J. Nucl. Mater.* 433 (2013) 174-179.

- 21 C. Heintze, F. Bergner, M. Hernández-Mayoral, Ion-irradiation-induced damage in Fe–Cr alloys characterized by nanoindentation, *J. Nucl. Mater.* 417 (2011) 980-983.
- 22 S. Ishino, Implications of fundamental radiation damage studies in the research and development of materials for a fusion reactor, *J. Nucl. Mater.* 239 (1996): 24-33.
- 23 R.S. Nelson, D.J. Mazey, J.A. Hudson, The use of ion accelerators to simulate fast neutron-induced voidage in metals, *J. Nucl. Mater.* 37.1 (1970): 1-12.
- 24 R.E. Stoller, G.R. Odette, B.D. Wirth, Primary damage formation in bcc iron, *J. Nucl. Mater.* 251 (1997) 49-60.
- 25 R. More, J. Spitznagel, Primary recoil spectra and subcascade effects in ion bombardment experiments, *Radiation Effects*. 60 (1982) 27-33.
- 26 R.E. Stoller, The role of cascade energy and temperature in primary defect formation in iron, *J. Nucl. Mater.* 276 (2000) 22-32.
- 27 E. Zarkadoula, S. Daraszewicz, D. Duffy, M. Seaton, I. Todorov, K. Nordlund, M. Dove, K. Trachenko, The nature of high-energy radiation damage in iron, *Journal of Physics: Condensed Matter*. 25 (2013) 125402.
- 28 H. Wiedersich, Effects of the primary recoil spectrum on long-range migration of defects, *Radiation effects and defects in solids*. 113 (1990) 97-107.
- 29 L. Rehn, Production of freely-migrating defects, *J. Nucl. Mater.* 174 (1990) 144-150.
- 30 J.L. Seran, J.M. Dupouy, Swelling of solution annealed 316 cladding in Rapsodie and Phenix, in: J.S.P. Brager (Ed.), *Effect of Radiation on Materials: 11th International Symposium*, ASTM, Baltimore, MD., 1982.
- 31 G.W. Lewthwaite, D. Mosedale, The effects of temperature and dose-rate variations on the creep of austenitic stainless steels in the dounreay fast reactor, *J. Nucl. Mater.* 90 (1980) 205-215.
- 32 C.D. Hardie, C.A. Williams, S. Xu, S.G. Roberts, Effects of irradiation temperature and dose rate on the mechanical properties of self-ion implanted Fe and Fe–Cr alloys, *J. Nucl. Mater.* 439 (2013) 33-40.
- 33 L.M. Brown and R.K. Ham, *Strengthening Methods in Crystals*, Applied Science Publishers, London (1971).
- 34 J.W. Martin, *Micromechanisms in particle-re-enforced alloys*, Cambridge University Press, 1980, p50.
- 35 W.D. Nix, H. Gao, Indentation size effects in crystalline materials: A law for strain gradient plasticity, *J. Mech. Phys. Solids*. 46 (1998) 411-425.
- 36 J.R. Greer, J.T.M. De Hosson, Plasticity in small-sized metallic systems: Intrinsic versus extrinsic size effect, *Progress in Materials Science*. 56 (2011) 654-724.
- 37 W.D. Nix, J.R. Greer, G. Feng, E.T. Lilleodden, Deformation at the nanometer and micrometer length scales: Effects of strain gradients and dislocation starvation, *Thin Solid Films*. 515 (2007) 3152-3157.
- 38 T.A. Parthasarathy, S.I. Rao, D.M. Dimiduk, M.D. Uchic, D.R. Trinkle, Contribution to size effect of yield strength from the stochastics of dislocation source lengths in finite samples, *Scr. Mater.* 56 (2007) 313-316.
- 39 C. Motz, T. Schöberl, R. Pippan, Mechanical properties of micro-sized copper bending beams machined by the focused ion beam technique, *Acta Materialia*. 53 (2005) 4269-4279.
- 40 D. Kiener, P. Hosemann, S.A. Maloy, A.M. Minor, In situ nanocompression testing of irradiated copper, *Nat Mater.* 10 (2011) 608-613.
- 41 ~~Tabor, David. *The hardness of metals*. Oxford university press, 2000. J.T. Busby, M.C. Hash, G.S. Was, The relationship between hardness and yield stress in irradiated austenitic and ferritic steels, *J. Nucl. Mater.* 336 (2005) 267-278.~~
- 42 Mansur, L. K. "Correlation of neutron and heavy-ion damage: II. The predicted temperature shift if swelling with changes in radiation dose rate." *Journal of Nuclear Materials* 78.1 (1978): 156-160.

**Formatted:** No Spacing

**Formatted:** Font: (Default) Calibri,  
Font color: Auto



[43] Hosemann, Peter, et al. "Issues to consider using nano indentation on shallow ion beam irradiated materials." *Journal of Nuclear Materials* 425.1 (2012): 136-139.

[44] Hardie, Christopher D., Steve G. Roberts, and Andy J. Bushby. "Understanding the effects of ion irradiation using nanoindentation techniques." *Journal of Nuclear Materials* 462 (2015): 391-401.

[45] T.Y. Tsui, G.M. Pharr, Substrate effects on nanoindentation mechanical property measurement of soft films on hard substrates, *J. Mater. Res.* 14 (1998) 292-301.

Table 1 - Elemental analysis provided by the manufacture and separate examination  
 | (compositions in weight percent). Data taken from ref.-~~[4][224]~~.

|                | Manufacturer | Chemical Analysis |
|----------------|--------------|-------------------|
| Cr             | 6.0          |                   |
| C              | 0.007        |                   |
| O <sub>2</sub> | 0.021        | 0.001             |
| N <sub>2</sub> | 0.0014       | 0.05              |
| P              |              | 0.005             |
| Ni             |              | 0.1               |
| Mn             |              | 0.02              |

Table 2 – Isotope activity measurements for Fe%6Cr sample irradiated in the ATR1 reactor at INL.. Data provided by Collin Knight (INL).

| Isotope | Curies   | MBq   |
|---------|----------|-------|
| HE 6    | 0.00E+00 | 0.0   |
| BE 8    | 0.00E+00 | 0.0   |
| B 12    | 0.00E+00 | 0.0   |
| C 14    | 3.34E-09 | 0.0   |
| SC 47   | 1.29E-18 | 0.0   |
| SC 48   | 2.00E-25 | 0.0   |
| SC 49   | 0.00E+00 | 0.0   |
| TI 51   | 0.00E+00 | 0.0   |
| V 52    | 0.00E+00 | 0.0   |
| V 53    | 0.00E+00 | 0.0   |
| V 54    | 0.00E+00 | 0.0   |
| CR 51   | 9.91E-04 | 36.7  |
| CR 55   | 0.00E+00 | 0.0   |
| MN 54   | 7.50E-04 | 27.8  |
| MN 56   | 0.00E+00 | 0.0   |
| MN 57   | 0.00E+00 | 0.0   |
| MN 58   | 0.00E+00 | 0.0   |
| FE 55   | 3.42E-03 | 127.0 |
| FE 59   | 1.88E-04 | 7.0   |
| CO 60   | 3.57E-05 | 1.3   |
| CO 60M  | 0.00E+00 | 0.0   |
| CO 61   | 0.00E+00 | 0.0   |
| Y 90    | 4.02E-15 | 0.0   |
| Y 90M   | 0.00E+00 | 0.0   |
| Y 91    | 2.50E-09 | 0.0   |
| TOTAL   | 5.38E-03 | 199.8 |

Table 3 - Ion beam conditions for implantation with multiple energies at the Ion Beam Center, Rossendorf.

|                    |        |                             |                                |
|--------------------|--------|-----------------------------|--------------------------------|
| Target Temperature | 288 °C | <a href="#">Ion species</a> | <a href="#">Fe<sup>+</sup></a> |
|--------------------|--------|-----------------------------|--------------------------------|

Formatted Table  
Formatted: Superscript

| Energy<br>(MeV) | Dose<br>(ions/cm <sup>2</sup> ) | Ion<br>Charge | Dose Rate<br>(ions/cm <sup>2</sup> /s) | Beam Current<br>(nA/cm <sup>2</sup> ) | Time (hrs) |
|-----------------|---------------------------------|---------------|--|---------------------------------------|------------|
| 0.5             | 1.16 x 10 <sup>14</sup>         | 1             | 1.60 x 10 <sup>10</sup>                | 2.56                                  | 2.02       |
| 1               | 2.18 x 10 <sup>14</sup>         | 1             | 1.84 x 10 <sup>10</sup>                | 2.95                                  | 3.29       |
| 2               | 2.18 x 10 <sup>14</sup>         | 1             | 2.00 x 10 <sup>10</sup>                | 3.21                                  | 3.03       |
| 3               | 2.18 x 10 <sup>14</sup>         | 1             | 2.16 x 10 <sup>10</sup>                | 3.46                                  | 2.80       |
| 4.5             | 2.18 x 10 <sup>14</sup>         | 2             | 2.38 x 10 <sup>10</sup>                | 7.62                                  | 2.55       |
| 6               | 2.91 x 10 <sup>14</sup>         | 2             | 2.31 x 10 <sup>10</sup>                | 7.41                                  | 3.49       |
| 9               | 8.00 x 10 <sup>14</sup>         | 3             | 2.34 x 10 <sup>10</sup>                | 11.24                                 | 9.50       |

|       |                         |
|-------|-------------------------|
| TOTAL | 2.08 x 10 <sup>15</sup> |
|-------|-------------------------|

|       |       |
|-------|-------|
| TOTAL | 26.69 |
|-------|-------|

Table 4 - Fitting parameters for *equation 6.1* and correlation coefficient *R*.

|                    | $A_0$ ( $\mu\text{mGPa}$ ) | $A_1$ (GPa) | $R$  |
|--------------------|----------------------------|-------------|------|
| Un-irradiated      | 2.43                       | 0.477       | 0.90 |
| Ion-irradiated     | 1.88                       | 1.16        | 0.94 |
| Neutron-irradiated | 3.79                       | 1.29        | 0.91 |

Table 5 Dislocation loops found in ion irradiated and neutron irradiated samples, and obstacle strength calculations.

|  | Ion irradiation [9]                                  |   | Neutron irradiation [9,10]                                |  |
|--|--|---|---|--|
|  | TEM  | APT   | APT   |  |
| Loop type                                | Mostly $\frac{1}{2}\langle 111 \rangle\{111\}$ -type | N/A   | Mostly $\frac{1}{2}\langle 111 \rangle\{111\}$ -type      |  |
| Segregating elements                     | N/A  | Si along the dislocation lines with lower C and P but no Cr | Cr enriched at the periphery, Si located inside the loops | Both Si and Cr outside the dislocation loops |
| Size (nm)                                | 6.4  | 9.2   | 9.2   | 18.1   |
| Number density (/ $10^{22}/\text{m}^3$ ) | 1.3  | 1.4   | 2.9   |  |
|  | <a href="#">Ion Irradiation (Current work)</a>       |   | <a href="#">Neutron Irradiation (Current work)</a>        |  |
| $\lambda$ (nm)                           | 100  | 80  | 41  | 32   |
| Mean $\lambda$ (nm)                      | 90   |   | 37  |  |
| $\Delta\tau_v$ (MPa)                     | 170  |   | 500   |  |
| $\phi_c$ (eqn 1)                         | 42°  |   | 26°   |  |
| $\phi_c$ (eqn 2)                         | 50°  |   | 32°   |  |

Dear Editor,

I would like to thank the reviewers for their extensive feedback. I have addressed all comments where possible and I have responded to individual issues in red below. I believe the revised manuscript has been much improved. Changes can be seen on the updated manuscript by track changes as recommended.

I think that this work is a unique study which reports on some interesting and important findings. I now hope that the revised manuscript will be considered for the journal of nuclear materials.

Best regards,  
Chris Hardie

Reviewers' comments:

Reviewer #1: I would recommend to restructure the paper in order to follow the logical flow of experiment, data discussion scientific discussion.

First the nanoindentation and micro cantilever test data are presented. Further the dose effects are discussed and only at the end comparisons between the different testing methods and macroscopic meaning is discussed. I would recommend to turn it around and first discuss the mechanical data and the plasticity aspects and then discuss where the discrepancies between neutrons and ions may come from.

OK: The order of discussion has now been changed.

Further detailed comments are below:

Introduction:

It would be better to differentiate and say that specific aspects of radiation damage can be simulated by ion beam damage.

I have added a sentence to acknowledge the differences between all types of irradiation and the importance of knowing these differences.

In recent times it was found that not all aspects of radiation damage can be simulated using ions. Already L. Mansur mentioned that different invariant temperatures should be used depending what defects are simulated and one cannot simulate all defects at the same time.

This theory was excluded from the original manuscript for the reason stated: all defects cannot be simulated by a single temperature shift. I have added a few lines to the discussion on dose rate to this effect.

The volume limitations of ion beam or neutron irradiated materials have been discussed in the literature comprehensively. It might be worthwhile citing the prior work in that area. More references in the introduction would give the reader a better perspective of the impact this work may have.

Agreed: I have added references specifically focused on the challenges of extracting mechanical properties of ion irradiated materials,

What was the volume of the neutron irradiated sample. To take full advantage of smaller sample size it is the mR/h/mm<sup>3</sup> which is the important factor to highlight. Just dose rate numbers by themselves are relatively meaningless in this context.

I have added the sample volume in the relevant section.

It appears to me that the authors performed the irradiation (neutron and ion) at the exact same temperature. Why was there no temperature offset applied for the ion beam irradiated samples as it is often practiced. L. Mansur provides the invariant equations to calculate the temperature which would account for the higher dose rate. G.S.Was and many others used this offset. If there is a specific reason this is not used please state and discuss.

The assessment of validity of temperature shift was not a focus of this work. As stated above a temperature shift can only be applied for a specific defect type and not the variety of defects induced as a result of irradiation. This subject is planned as future work.

Table 3: please provide the ion species in the table capture. Done.

Ion beam experimental section: Was the beam raster or broad beam? Did you have a homogeneous beam profile or a Gaussian current distribution over the sample surface? It may be worthwhile citing previous work which have more experimental details on the ion beam irradiation at this facility.

I am afraid that I do not have a reference with more detail, however I have added additional information.

Please provide amplitude and frequency for the CSM method used. Done.

For equation 1 and 2 references may be needed or a more detailed explanation. The equations are different from Miao and Roberts (J. Mat Res. 2005) it appears.

I have added to the sentence to explain how the equation is derived (from simple beam theory).

It is stated: "Post-indentation contact area measurements of all indent impressions in the un-irradiated and neutron irradiated material were conducted by SEM imaging (figure 5)."

How is the contact area obtained from SEM? Would AFM not be more suitable? More detail is needed on how you correct for the contact area using SEM images. More detail added to explain the techniques used. AFM imaging was not possible for this work and previous use of AFM has proved less successful.

In Figure 4a and 4b it is a bit difficult to see the corrected data. Maybe mark the data points in the graph for clarity. It would be worthwhile mentioning that you can only do the correction for the 1000nm values since this is final imprint. This leaves me wonder if one could apply an extrapolated correction to all the other data points. I have added to the graph and caption to improve clarity. I have also thought about post correction of the data using stiffness response following post indent measurement of contact area for validation; however this is work in progress!

I assume you are plotting the elastic modulus of the material not the reduced modulus?

It is stated: "almost perfectly plastic response." Do you mean "ideal plastic behavior"? I meant no increase in stress following yield, but I have removed as the statement was confusing.

You are stating: "For the ion irradiated material, there is good agreement between the TEM and the APT measurements for the number density of loops: 1.3 to 1.4x10<sup>22</sup> m<sup>-3</sup>.



How do the authors in the cited reference measure loop number density using APT? Are they measuring the elemental segregation around loops? It would be worthwhile mentioning what exactly is measured and compared. I completely agree. These details are not known. It has been difficult to get data from this work; hence we can only cite what is out in the literature.

You are reporting 1000MPa proof stress of the unirradiated material. How does this compare to a tensile test and the indentation data? The deep indents (1000nm) seem to show a hardness of 2GPa while the proof stress reported is 1GPa. There is a short discussion on this topic at the end. However, it might be worthwhile to expand the discussion and putting it before the dose calc. discussion since it speaks to the measured data directly and would be a worthwhile discussion for the community. The order of discussion has been changed. I have added a sentence describing the nanoindentation results subject to same calculation as the Vickers hardness. The numbers appear to be quite similar to the cantilever data which is interesting and suggests that there is an indentation size effect which is to be expected.

Thank you on the nice discussion of dose calculations and PKA spectrum this is well received. It would be great if you can add how this discussion ties in with L. Mansur's temperature invariant equations. I have referred to the work of L Mansur in the dose rate discussions, however I do not feel confident in discussing how this ties in with the dose calculation and PKA effects other than they are not accounted for?! I'm not fully familiar with the theory (although I would like to be). Additional information on how these effects are tied would be very much appreciated.

Reference is needed" we take hardness as being  $\sim 3\times$  (tensile) yield stress, and shear flow stress as being  $\frac{1}{2}$  the yield stress." Why? I have added the reference and explanation required for this. Reference for Equ 11. Done.

Page 20 discusses pop in events. In the data presented no pop in events are shown or discussed prior to this statement. Did you see any or do you refer to literature reports. It is sometimes difficult to see what results from the data here and what is based on the literature. I have added clarification to the sentence.

Table 5 is somehow confusing. This is data from reference 9 and 10. But in the text it states  $\phi(c)$  is calculated from the nanoindentation data. It is not clear what comes now from the nanoindentation data and what comes from the reference. Agreed. I have added a row to show that the bottom half of the table is from current work.

The first observation of size effect at least for indentation is from F. Schulz and H. Hanemann in Z. Metallkunde 33(1941) 124. However, this article is difficult to obtain. Thank you for this information I was not aware of this work. I haven't changed the text since it discusses tensile strength so should be valid still. I shall try to access the article by Schulz et al.

Reviewer #2: Title→ This manuscript doesn't contain any microstructural characterization. Unfortunately this data was not possible to include directly in the paper. I have changed the title. - Abstract → "The materials were characterised by Transmission Electron Microscopy (TEM) and Atom Probe Tomography (APT); "TEM and APT results identified that the dislocation loop densities were  $\sim 2.9 \times 10^{22} \text{m}^{-3}$  for the neutron irradiated material and only  $\sim 1.4 \times 10^{22} \text{m}^{-3}$  for the ion irradiated material."; "Cr segregation to loops was only found for the neutron-irradiated material."→ There are no APT and TEM investigations in this paper. Only references to a report and a publication. I have

amended the abstract to clarify what is new work and what is reported elsewhere. The data reported elsewhere is integral to the interpretation and discussions of the paper.

- 'This produced the microstructure shown in figure 1' → please describe the microstructure and use a better quality picture. Is the microstructure ferritic, martensitic, bainitic? Ref [10] describes the structure as coarse ferrite but what is the grain size. This is also important as it is for example stated in section 3.2 'As the beam size increases, more grains contribute to the elastic modulus. An EBSD overview picture might be helpful in justifying this statement. It is unfortunate that this is the only information I have. Additional EBSD work would be feasible but would delay the publication of this work further.

Section 2.2 → how is the second paragraph relevant for the current work? Activity data is very useful for those who are considering similar work. The information also adds evidence to the theme that n-irradiated samples can have limited volumes to allow work in a university environment.

-Section 2.4:

--What does depth from 0.82 to 7.30 μm; 0.36 to 2.3 μm; 0.53 to 5.11 μm mean? Is depth the same as height in Fig. 6? --What are the actual dimensions of the beams/cantilevers? Was there an anticipated ratio like e.g. cross/section to length, height to length, depth to length? Yes depth should say 'cross-sectional height. I have changed the wording to improve clarity.

--What were the cutting parameters? How was the irradiation damage due to the FIB beam taken in to account? I have added a sentence to describe the general approach. FIB damage is expected to reside within a ~6nm outer layer as calculated by TRIM in work elsewhere. The damage would have been present for all beams and would have a minimal and identical effect on all beams.

-Section 3.3 → This section should be removed. Microstructure is not discussed in this manuscript. Only results from other investigations are repeated. This section provides necessary information for the discussion.

-Section 4.4 → Regarding the statement "According to the empirical relationships derived for irradiated austenitic and ferritic steels [41], dividing these values by 3.03 provides an estimate of the macro scale yield stress..". In the referred publication it is: - it's multiplying; - it's not about absolute values of yield strength, it's about the relation between the change of hardness and the change of yield strength, - the found factor in reference [41] is 3.06 for ferritic steels. This is a simple method for correlation for the purpose of comparison, however I accept that the reference was not for absolute values of yield stress. I have changed the reference to cite the traditional work and simplified the factor to 3.

Table 1: 'Data taken from ref. [224]' → there is no reference 224 corrected.

Fig 1: At least in the received .pdf document this is a really bad quality picture; How was the microstructure sample prepared? Was the sample etched? If yes ... how? I agree that this picture is bad quality. It is a simple optical microscope image and the sample was etched as suggested in the caption. This is the extent of information available for this image. I am afraid that this is all that is possible at present.

Fig. 11: Dierckx [118] → there is no reference 118 corrected

Cosmetics:

-There should be a space between number and SI unit -The acronyms FEA, SEM are never introduced -The acronyms ENS, CAES are introduced but never used Thank you I have amended the text throughout

-Some questions:

--Typically YS and UTS of ferritic and martensitic alloys tend to saturates at a neutron dose of around 7-10 dpa. How does this compare to the statement: "However, several ion implantation studies of a similar alloys have identified that irradiation hardening saturates at a doses of 1-2dpa"? Does this mean that 1-2 dpa compare to 7-10 dpa in neutron irradiation or that ion-irradiation can only imitate neutron irradiation up to 1-2dpa. I believe this is due to the difference in dose rate. **The faster the dose rate the less time point defects have before they agglomerate with like defects or are annihilated by other defects or sinks. It may be that a steady state microstructure is formed at lower doses in ion irradiation than in neutrons. Also, irradiation of a binary alloy is less complex than a steel.**

--The intention of ion-irradiation is to simulate neutron irradiation. If there is a difference of a factor of 3 between ion-and neutron irradiation for the 'same' dose, isn't this a sign that one or the other dose calculation is not accurate enough (or that the recommendation of Stoller should be followed) or that ion-irradiation can't simulate neutron irradiation damage? **This is discussed in the paper extensively. The difference may be one or more of a number of things.**

--Doesn't the loop density also suggest that the dose for the ion-irradiated material was only half of the anticipated dose? **It could be, but loop sizes are different. I think it is too simplistic to relate this to dose alone because it assumes that the fraction of surviving defects are the same for both irradiation types and this is not likely.**

I recognize that the presented data is unique and a large amount of work. I also consider publishing of experimental data as very important. Nevertheless, in the current form I do not understand the intention of the manuscript. While in the title and the abstract microstructural characterizations are pointed out, the only 'microstructure characterization' is given by a low quality light microscope picture and the repetition of results from a DOE report. Furthermore, I think that the inconsistencies in dose calculation need more attention. Therefore, I recommend resubmission after thorough rework.

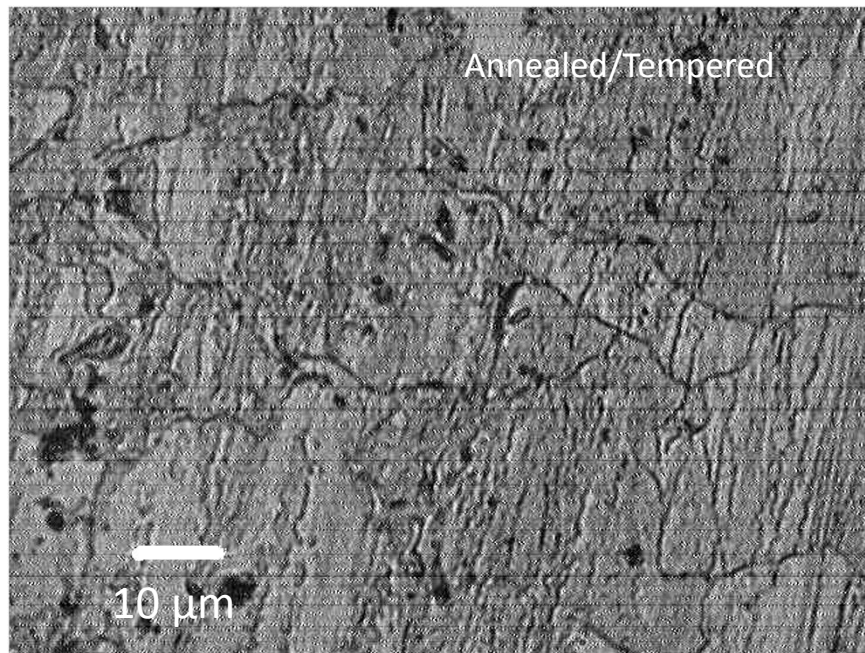


Figure 1 –Optical microscopy image of the microstructure of Fe 6%Cr after anneal and temper. Sample polished and etched.

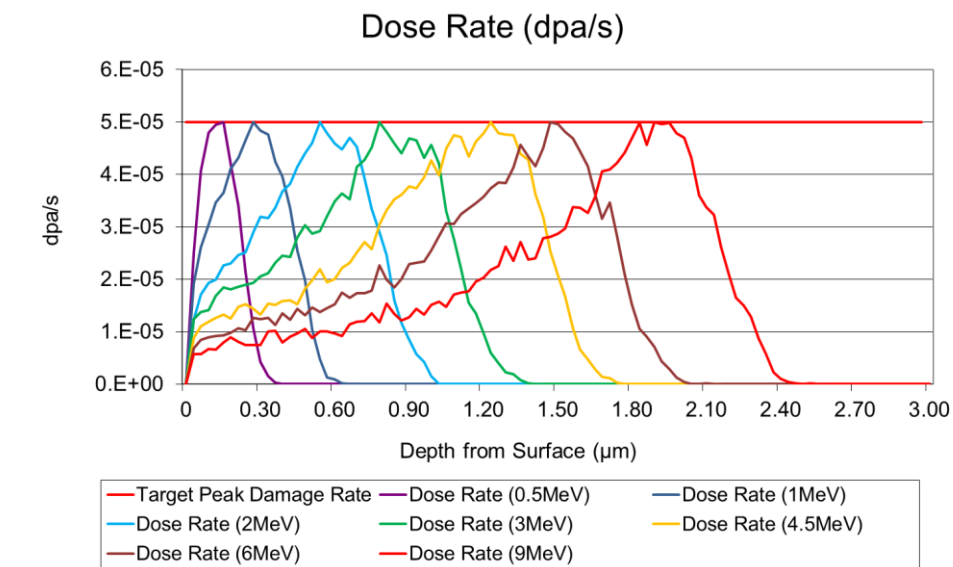
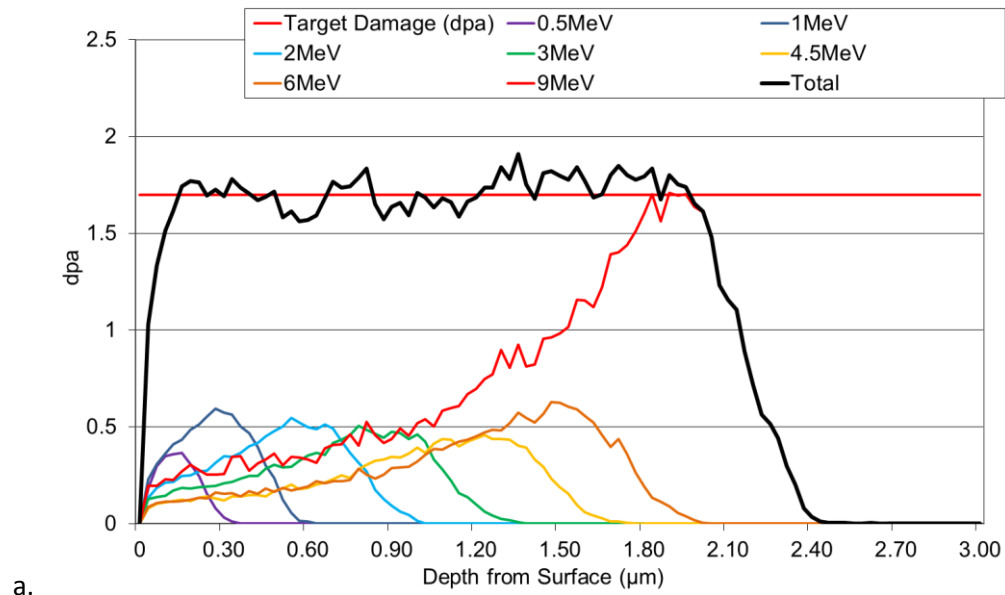


Figure 2 - SRIM calculations showing (a) irradiation damage from iron ions vs. depth into sample surface, including total damage and contributions from each beam energy, and (b) dose rate vs. depth into sample surface for each energy.

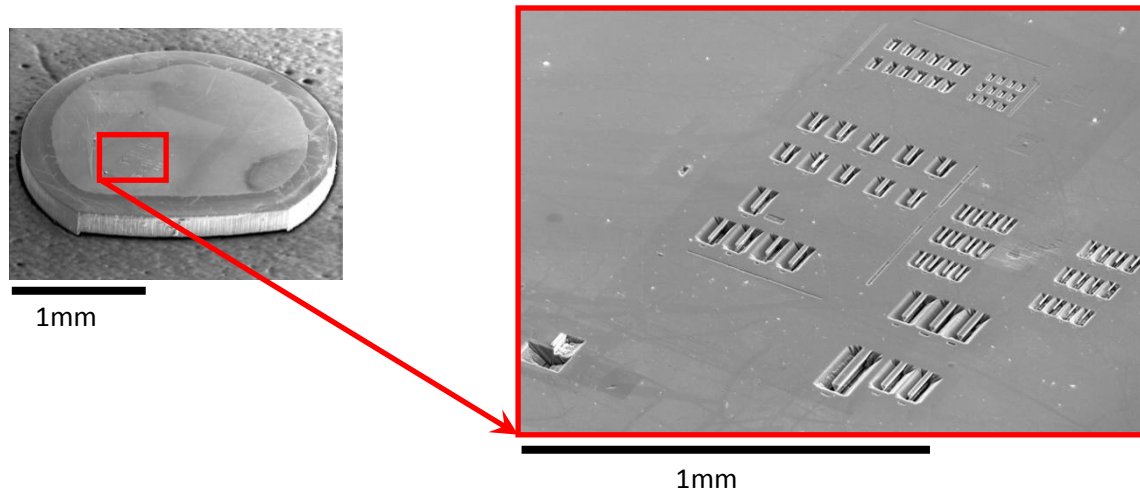
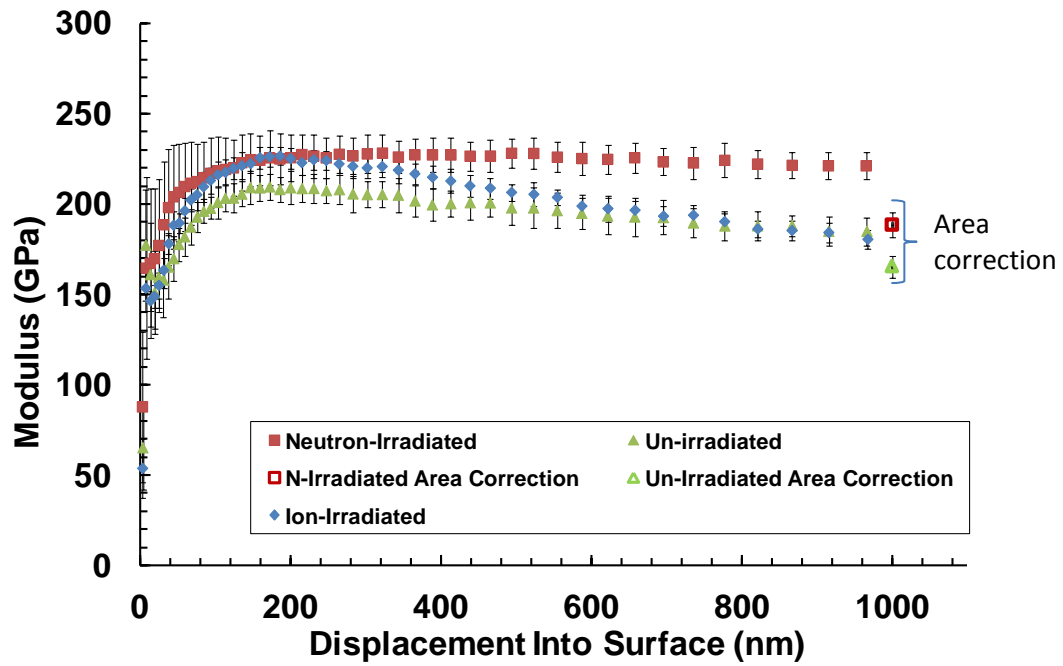
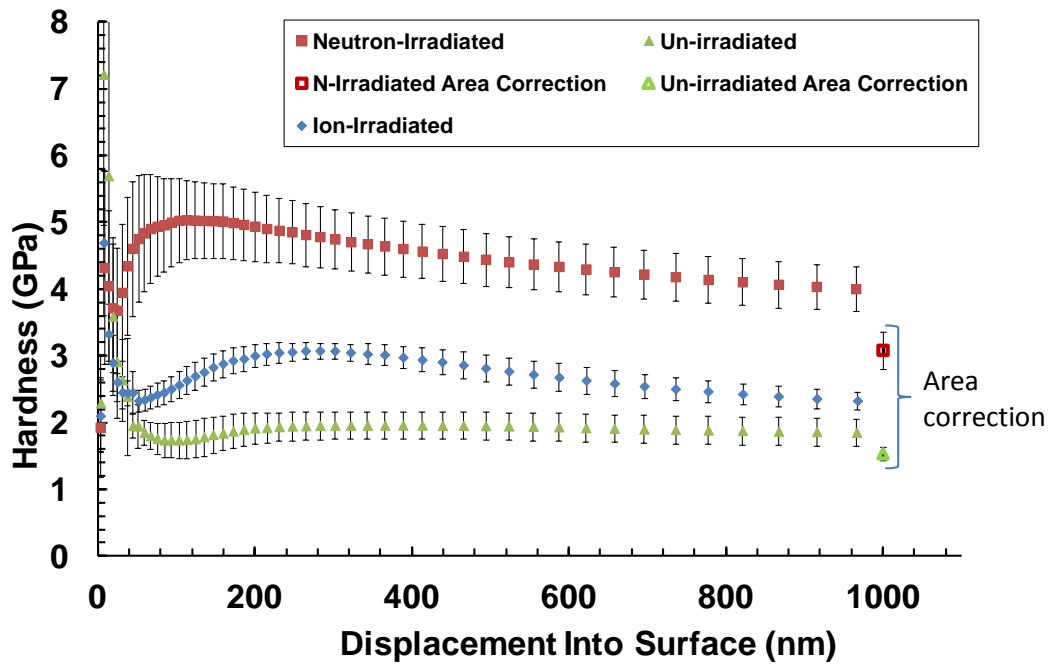


Figure 3 – SEM micrographs showing entire neutron irradiated sample (left) and region of arrays of micro-cantilevers of various sizes (right).



a.



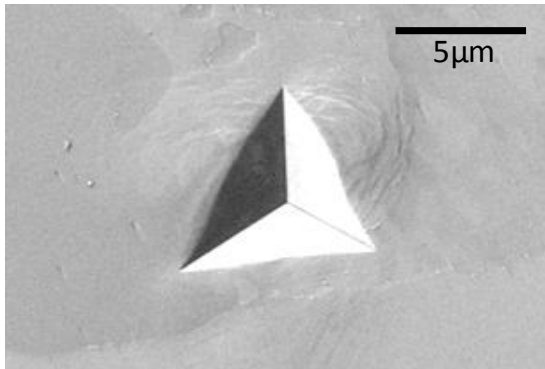
b.

Figure 4 – (a) Average elastic modulus and (b) hardness versus indentation depth for arrays of at least 16 indents produced in each of the un-irradiated, ion-irradiated and neutron irradiated Fe 6%Cr specimens. Error bars represent +/- one standard deviation. For the un-irradiated and neutron irradiated condition, data at maximum displacement has been

corrected to account for pile-up of material surrounding the indenter tip from post indent contact area measurements.



**UN-IRRADIATED**



**NEUTRON-IRRADIATED**

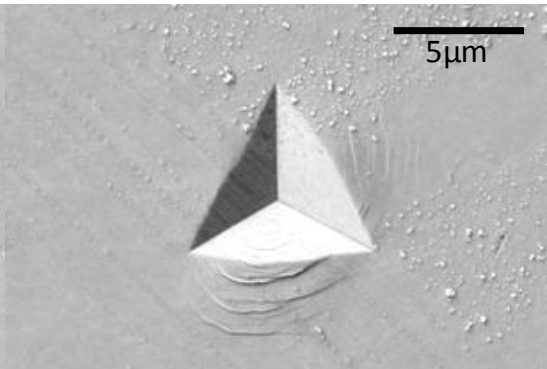


Figure 5 – SEM micrographs of typical indent impressions in the un-irradiated and neutron irradiated material.

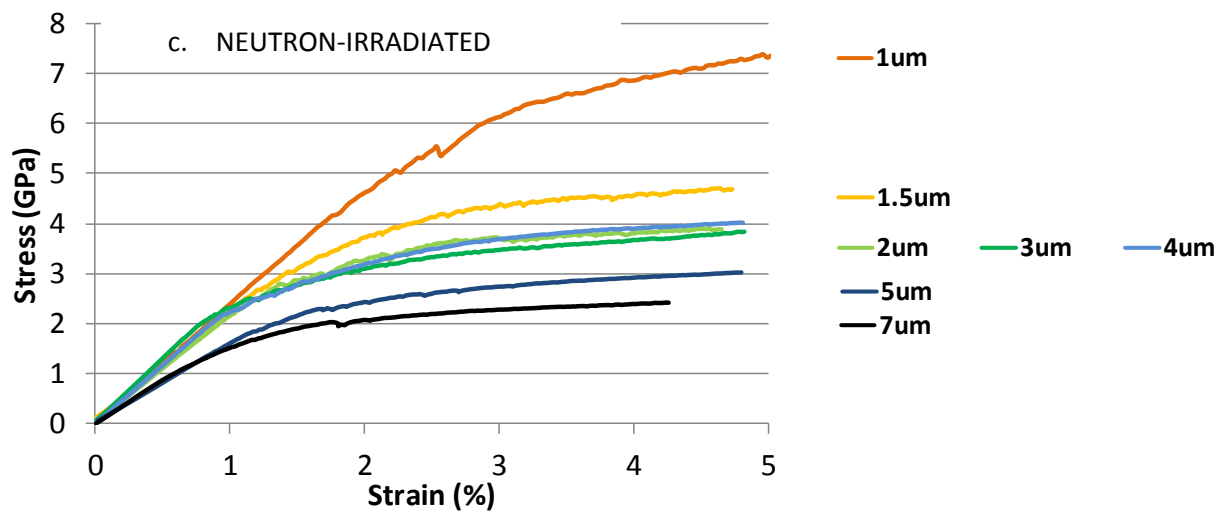
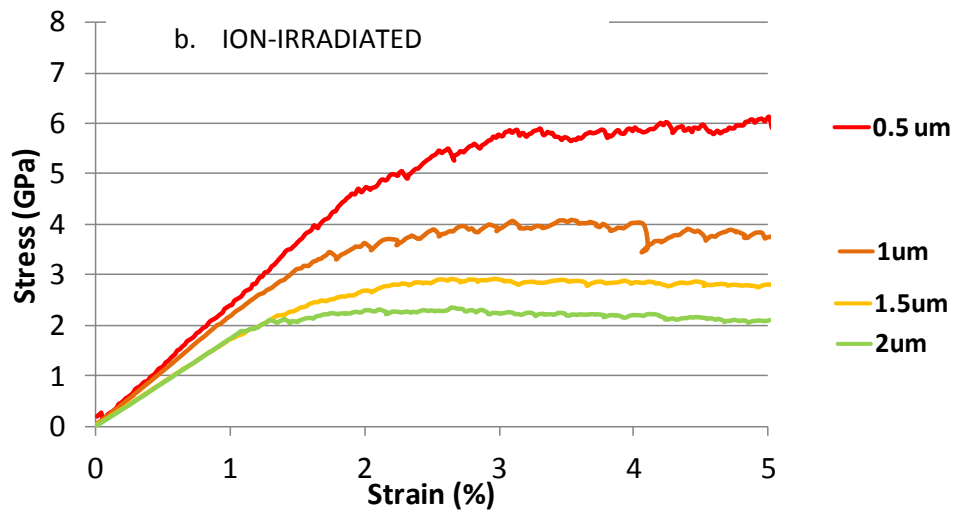
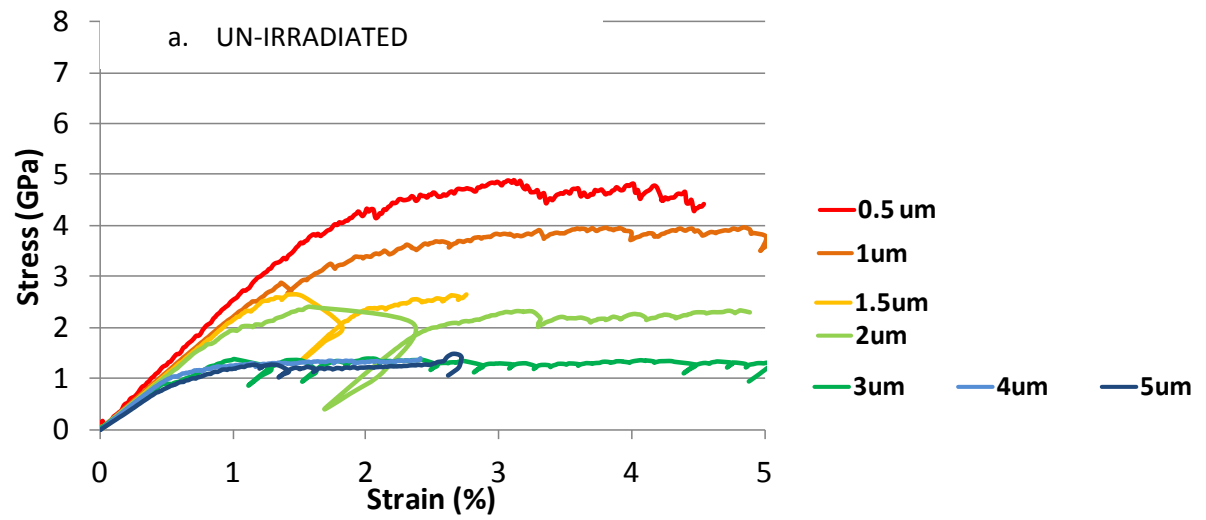


Figure 6 - Typical stress-strain curves from micro-cantilever tests of various sizes in: (a) un-irradiated, (b) ion-irradiated and (c) neutron irradiated material. Various rounded beam heights shown with different colours.

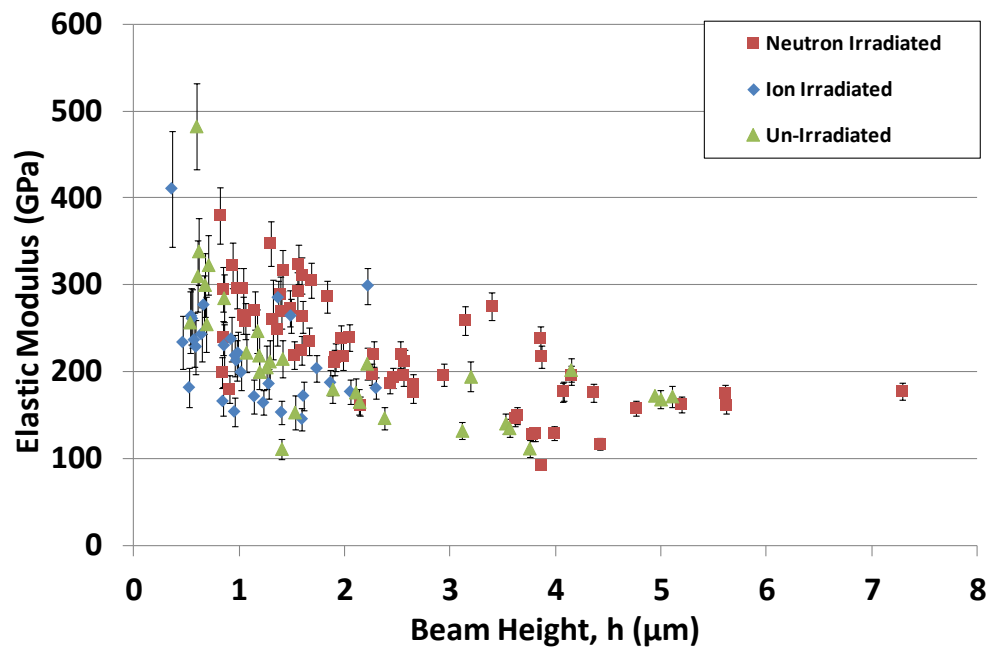


Figure 7 - Elastic modulus measurements versus beam height,  $h$ , for all micro-cantilevers tested in the un-irradiated, ion-irradiated and neutron-irradiated material. Error bars represent estimated error according to analysis reported in *section 2.4*.

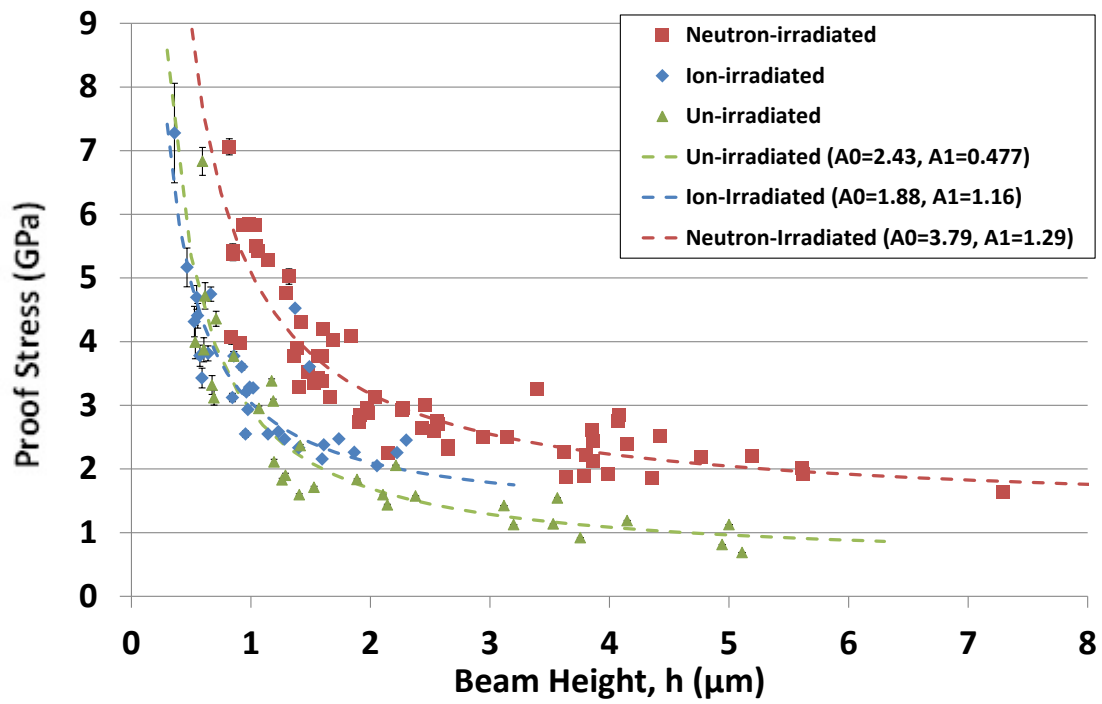


Figure 8 - Proof stress measurements versus beam height,  $h$ , for all micro-cantilevers tested in the un-irradiated, ion-irradiated and neutron-irradiated material. Error bars represent estimated error according to analysis reported in *section 2.4*.

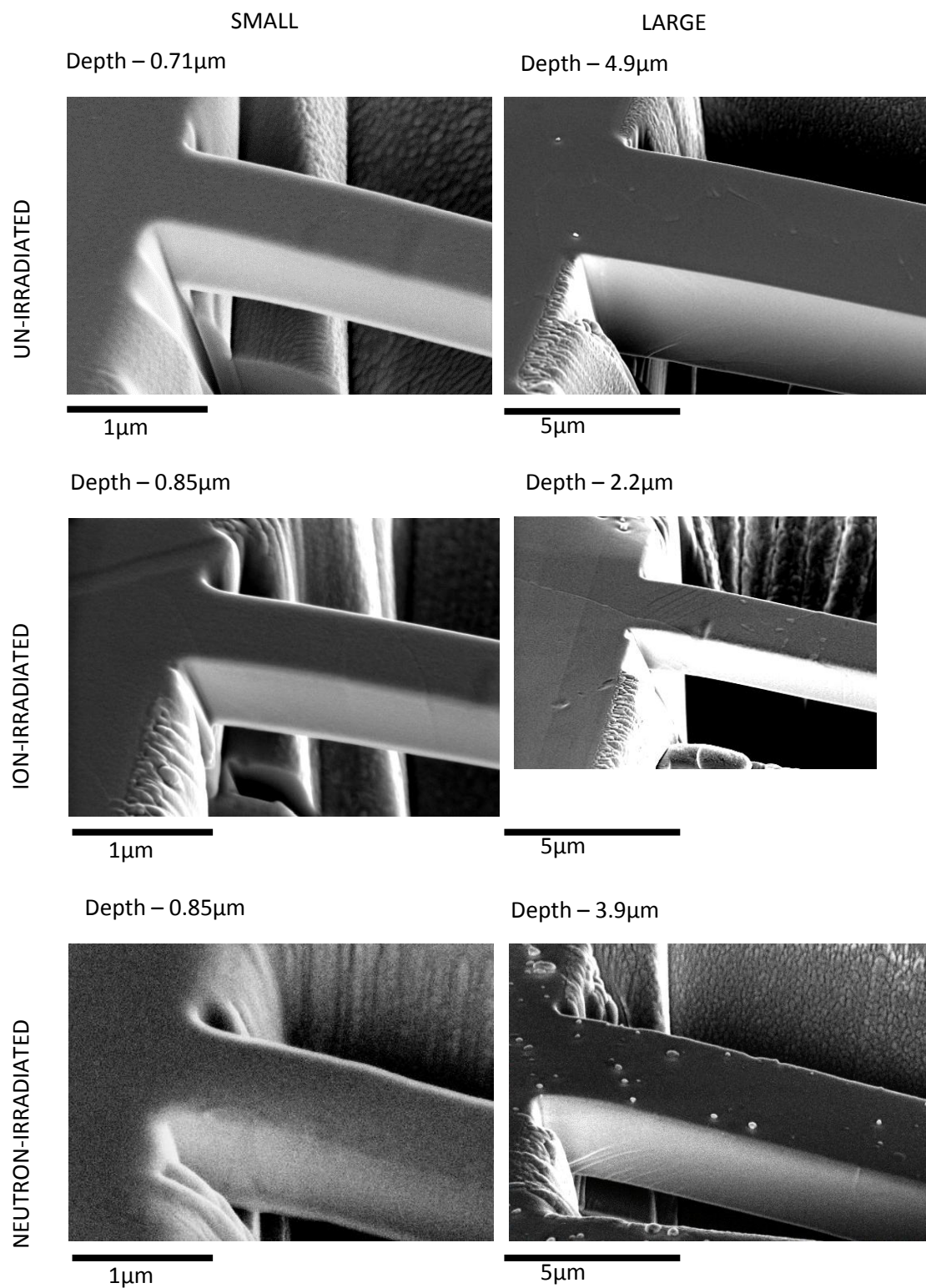


Figure 9 - Typical SEM micrographs of plastic deformation on the surfaces of micro-cantilever beams tested in the un-irradiated, ion-irradiated and neutron-irradiated beams.

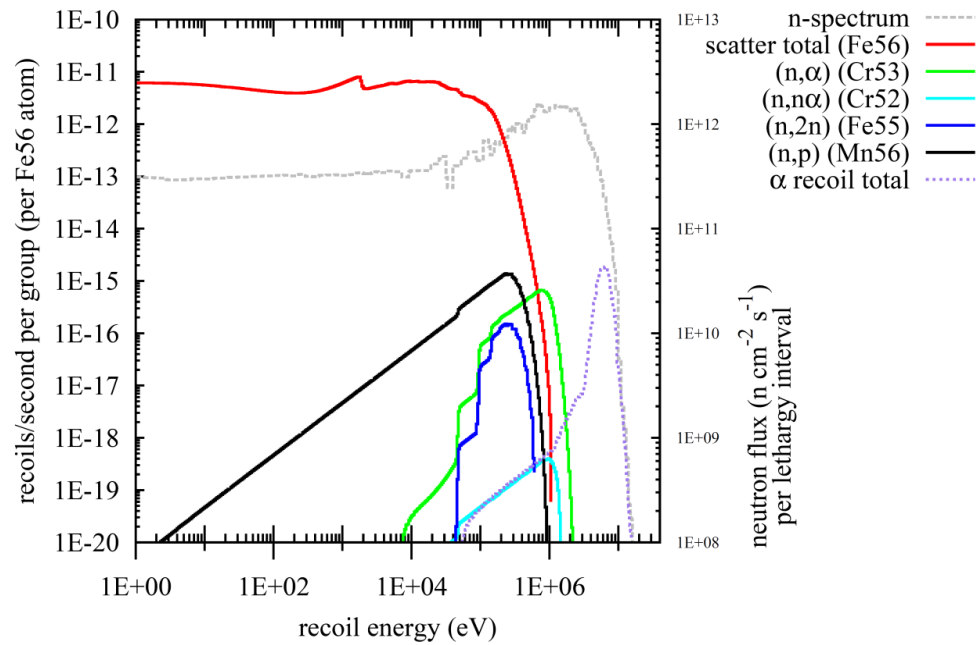


Figure 10 - PKA energy spectra for dominant reactions in the ATR1 reactor. Data produced by Dr M Gilbert (CCFE).

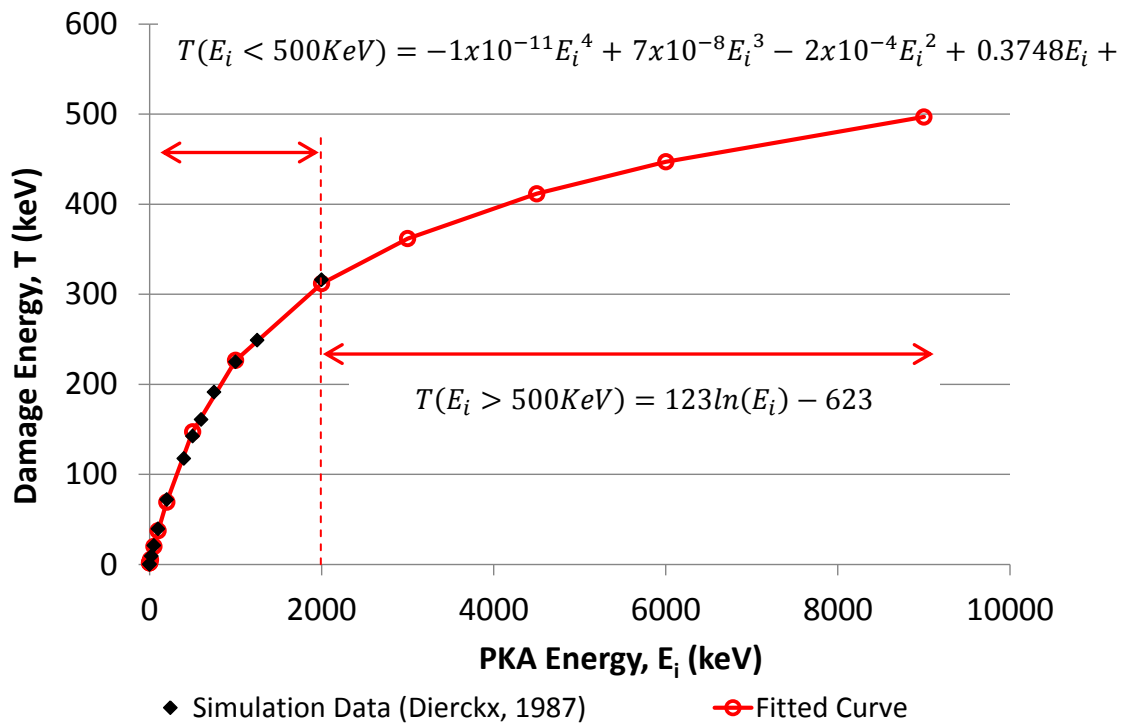


Figure 11 - Damage energy,  $T$ , as a function of PKA energy,  $E_i$ , in iron modelled using the data and relationships produced by Dierckx [17].

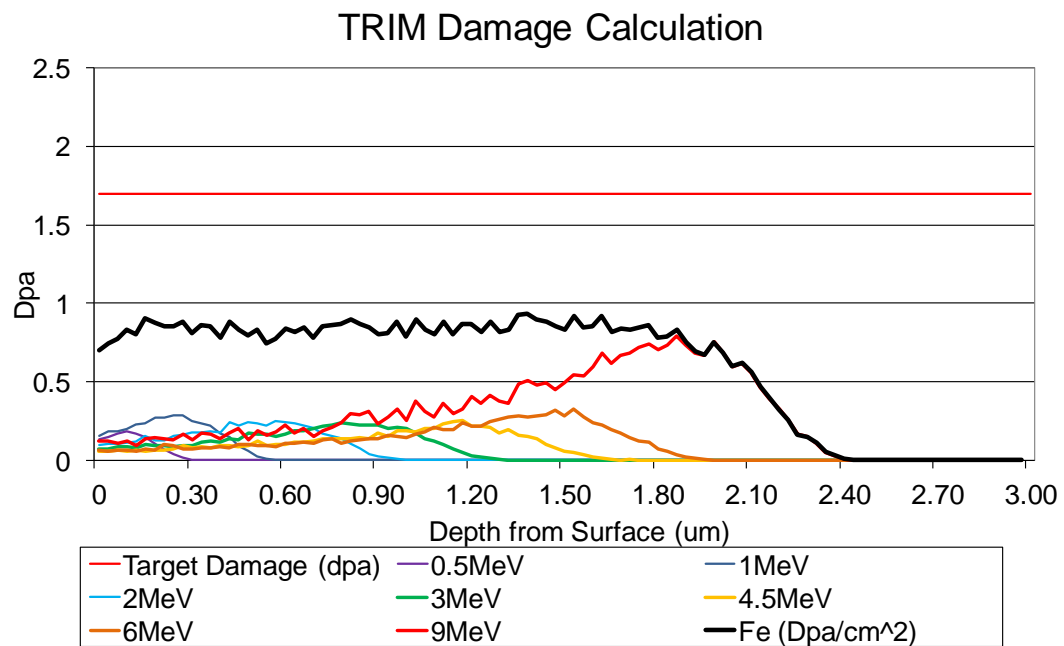


Figure 12 – SRIM calculations based on the Kinchin and Pease model showing irradiation damage vs. depth into sample surface, including contributions from each beam energy and total damage.



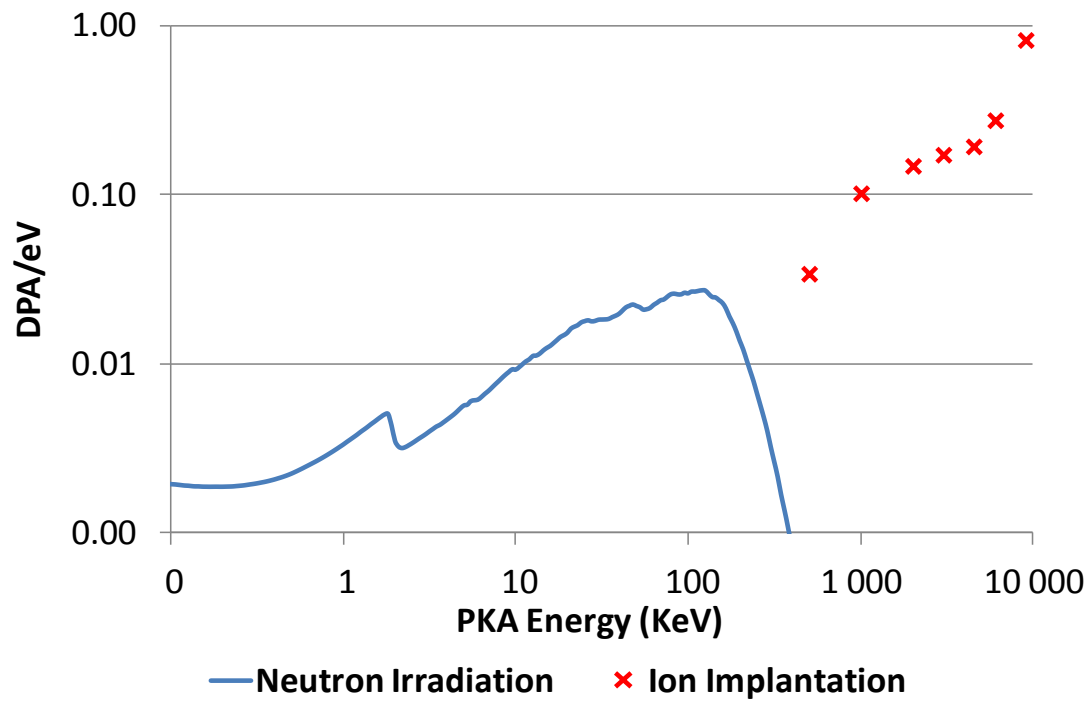


Figure 13 – Radiation damage as a function of PKA energy for ion and neutron irradiations. See text for details.